eLife

Reviewed Preprint
v2 • October 16, 2025
Revised by authors

Reviewed Preprint
v1 • December 2, 2024

Neuroscience

Dependence of Contextual Modulation in Macaque V1 on Interlaminar Signal Flow

Shude Zhu, Yu Jin Oh, Ethan B Trepka, Xiaomo Chen, Tirin Moore

Department of Neurobiology and Howard Hughes Medical Institute, Stanford University School of Medicine, Stanford, United States • Center for Neuroscience, Department of Neurobiology, Physiology, and Behavior, UC Davis, Davis, United States

eLife Assessment

The results by Zhu et al provide **valuable** insights into the representation of border ownership in area V1. They used neuropixel recording to demonstrate the clustering of border ownership, and compared cross-correlation functions between neurons in different layers to demonstrate that they depend on the type of stimulus. The strength of the evidence is **solid** but can be improved by performing additional analyses and addressing some concerns (as raised in the previous and current review), and accounting for the differences in classical and non-classical receptive field stimulation conditions.

https://doi.org/10.7554/eLife.103255.2.sa4

Abstract

In visual cortex, neural correlates of subjective perception can be generated by modulation of activity from beyond the classical receptive field (CRF). In macaque V1, activity generated by nonclassical receptive field (nCRF) stimulation involves different intracortical circuitry than activity generated by CRF stimulation, suggesting that interactions between neurons across V1 layers differ under CRF and nCRF stimulus conditions. Using Neuropixels probes, we measured border ownership modulation within large, local populations of V1 neurons. We found that neurons in single columns preferred the same side of objects located outside of the CRF. In addition, we found that cross-correlations between pairs of neurons situated across feedback/horizontal and input layers differed between CRF and nCRF stimulation. Furthermore, independent of the comparison with CRF stimulation, we observed that the magnitude of border ownership modulation increased with the proportion of information flow from feedback/horizontal layers to input layers. These results demonstrate that the flow of signals between layers covaries with the degree to which neurons integrate information from beyond the CRF.

Introduction

The classical receptive field (CRF) defines the region of the sensory periphery where appropriate stimulation evokes a spiking response in a neuron (Hartline, 1938; Alonso and Chen, 2009). Those evoked responses are largely driven by feedforward inputs from earlier stages of sensory processing. In macaque primary visual cortex (V1), neuronal activity is largely determined by ascending input from the dorsal lateral geniculate nucleus (dLGN) which arrives principally in layers 4Cα and 4Cβ (Hubel and Wiesel, 1972; Hendrickson et al., 1978; Blasdel and Lund, 1983; Callaway, 1998; Callaway, 2004). However, considerable evidence has established that the responses of sensory cortical neurons are also robustly influenced by stimulation concurrently presented outside of the CRF (Allman et al., 1985; Fitzpatrick, 2000; Albright and Stoner, 2002; Roelfsema, 2006; Angelucci et al., 2017). Specifically, whereas stimulation outside of the CRF alone fails to evoke spiking responses, such stimulation nonetheless alters the responses evoked by stimulation within the CRF. In visual cortex, these nonclassical receptive field (nCRF) effects often contribute to the neural correlates of visual perceptual phenomena, such as illusory contours (von der Heydt et al., 1984; Ramsden et al., 2001), visual salience and boundary segmentation (Knierim and van Essen, 1992; Sillito et al., 1995; Yan et al., 2018; Lee et al., 2002; Nothdurft et al., 1999), contour integration (Nelson and Frost, 1985; Kapadia et al., 1995; Li et al., 2006), figure-ground segregation (Lamme, 1995; Zipser et al., 1996; Poort et al., 2012), and border ownership (Zhou et al., 2000; von der Heydt, 2015; von der Heydt, 2023).

In contrast to the feedforward mechanisms underlying the CRF, nCRF effects are thought to be generated either by feedback from neurons with larger CRFs in higher areas (Hupe et al., 1998; Bullier et al., 2001; Bair et al., 2003; Nassi et al., 2013; Chen et al., 2017; Klink et al., 2017; Zhang et al., 2014; Nurminen et al., 2018; Keller et al., 2020; Pak et al., 2020; Vangeneugden et al., 2019; Gieselmann and Thiele, 2022; Chen et al., 2014; van Kerkoerle et al., 2014), or through intracortical horizontal connections (Adesnik et al., 2012; Chisum et al., 2003; Stettler et al., 2002), or by both (Angelucci and Bressloff, 2006; Schwabe et al., 2006; Ichida et al., 2007; Angelucci et al., 2017; Liang et al., 2017; Self et al., 2013). In contrast to feedforward inputs, feedback and horizontal inputs to V1 both avoid layer 4C and terminate predominantly in superficial (layers 1-3) and deep (layers 5-6) layers (Rockland and Lund, 1983; Rockland and Pandya, 1979; Rockland and Virga, 1989; Anderson and Martin, 2009; Markov et al., 2014; Federer et al., 2021; Gilbert and Wiesel, 1983; Shmuel et al., 2005; Siu et al., 2021). These differences between feedforward and feedback/horizontal circuitry suggest that the flow of signals across V1 layers should covary with the type of visual stimulation.

Newly developed, high-density Neuropixels probes have enabled recordings from a large, dense population of neurons (Jun et al., 2017; Zhu et al., 2024; Trautmann et al., 2025), and dramatically increase the quantity of identifiable functional interactions between pairs of neurons, particularly in non-human primates (Trepka et al., 2022). Recently, this approach was used to recapitulate known circuit properties, such as the pairwise lead-lag relationship between simple and complex cells and the canonical laminar input-output relationship in macaque V1 (Trepka et al., 2022), as well as the visual hierarchy in mouse visual cortical (Siegle et al., 2021; Jia et al., 2022) and subcortical areas (Sibille et al., 2022).

Here, using Neuropixels probes, we recorded the activity of hundreds of neurons simultaneously from single V1 columns in anesthetized macaques during CRF and nCRF stimulation. We leveraged the high yields obtained from different layers to examine the organization and circuitry underlying contextual modulation, specifically border ownership (B_{own}). B_{own} is a form of contextual modulation in which neurons signal the occluding border between the background and a foreground object using stimulus information beyond the CRF. This function appears to be

crucial for natural scene segmentation and object recognition (Nakayama et al., 1995). It has been shown that many neurons in early visual areas, including V1, respond differently to identical edges (borders) of objects when those objects lie at different locations outside the CRFs (Zhou et al., 2000; Franken and Reynolds, 2021; Hesse and Tsao, 2016; Hesse and Tsao, 2023). B_{own} emerges rapidly after visual response onset (Sugihara et al., 2011), yet the relative contributions of feedforward, feedback, and horizontal circuits to B_{own} remain unknown. Also unknown is whether B_{own} is present under anesthesia. Several other types of contextual modulation have been demonstrated in anesthetized animals (Ramsden et al., 2001; Hupe et al., 1998; Bair et al., 2003; Allman et al., 1985; Gilbert and Wiesel, 1990; Nothdurft et al., 1999; Webb et al., 2003; Zarella and Ts'o, 2016; Muller et al., 2003; Henry et al., 2013; Bijanzadeh et al., 2018; although see Lamme et al., 1998) and can involve inter-cortical feedback (Nurminen et al., 2018). Moreover, B_{own} has been shown to occur independently of attention (Qiu et al., 2007; O'Herron and von der Heydt, 2009), and before object shape recognition (Williford and von der Heydt, 2016; Ko and von der Heydt, 2018), suggesting it may not rely on higher cognitive control or object recognition areas. Rather, B_{own} may emerge through pre-attentive, automatic grouping mechanism in low/middle level visual areas, signifying a representation of "proto-objects" in the early visual cortex (von der Heydt, 2015; von der Heydt, 2023; Self et al., 2019).

Results

Classical RF stimulation in single V1 columns

Neuronal activity was recorded from two anesthetized rhesus macaques (M1 and M2, *Macaca mulatta*) using high-density, multi-contact Neuropixels probes (version 3A, IMEC Inc., Belgium) (**Figure 1A**) (Methods). These animals had no prior experience with awake experiments or exposure to the stimuli used in this study. Neuropixels probes were inserted into the lateral operculum of V1 with the aid of a surgical microscope at angles nearly perpendicular to the cortical surface. Prior to insertion, the probes were coated with a DiI derivative for subsequent histological visualization of the tracks (Methods) (**Supplementary Figure S1**). Four Neuropixels probe penetrations were made either in the opercular surface (M1, *pen 1-2*, ~4-6° eccentricities) or within the underlying calcarine sulcus (M2, *pen 3-4*, ~6-10° eccentricities) using the programmable channel selection feature of the Neuropixels probe. The boundaries of laminar compartments were estimated by combining current-source density (CSD) measurements and histological data (**Figure 1B**; **Supplementary Figure S1**) (Methods) (Zhu et al., 2024; Carr et al., 2025). Each recorded neuron was assigned to one of four laminar compartments, specifically 5/6, 4C, 4A/B, 2/3 (mean thickness: 489, 281, 311, 650 μm, respectively, consistent with previous anatomical (O'Kusky and Colonnier, 1982; Lund, 1973) and CSD (Self et al., 2013; Chen et al., 2017) studies). We measured the responses from a total of 677 visually driven neurons (N = 159, 181, 210, and 127 per recording) to classical receptive field (CRF) stimulation, and 621 neurons (N = 142, 179, 152, and 148 per recording) to nonclassical receptive field (nCRF) stimulation (Methods). As a result of the nearly perpendicular penetrations, the visual CRFs of V1 neurons were largely overlapping across the cortical depth (**Figure 1C**).

During each recording session, neurons were first tested with CRF stimuli consisting of drifting Gabor gratings with 1.5 degrees of visual angle (dva) in diameter, presented at the joint CRF location of simultaneously recorded neurons (Methods). In each of the four recordings, neurons across cortical depth exhibited very similar preferences to grating orientations (**Figure 1D**). The modal pairwise difference in preferred orientation between neurons across layers was near zero (*pen1* = 5°; *pen2* = 5°; *pen3* = 1°; *pen4* = 1°). This result confirmed that our recordings were nearly perpendicular and included neurons predominantly from single orientation columns. Gratings were sized to largely restrict the stimuli within the CRFs of recorded neurons to maximize the extent to which V1 responses were driven in large proportion by feedforward circuitry. In V1,

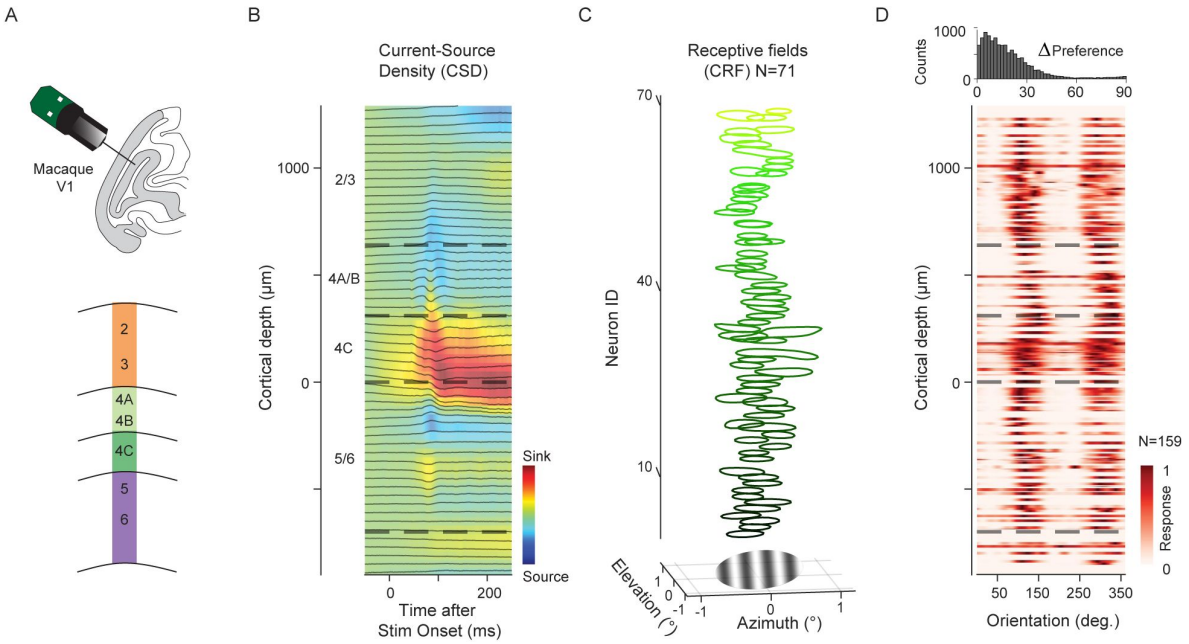

Figure 1.

Classical receptive field (CRF) stimulation in single V1 columns

(A) Neuropixels probe (384 channels/3.84mm) penetrations made into the lateral surface or underlying calcarine sulcus of macaque V1. Bottom: Diagram of designated laminar compartments. (B) Current-Source density (CSD) profile from an example recording session (M1, *pen1*), showing the early current sink (red) indicative of layer 4C. Laminar compartment boundaries (dashed lines) were determined using histological data and the CSD profile. (C) Top: 71 well-defined classical receptive fields (CRF) vertically stacked along the cortical depth, mapped with a 10 x 10 array (4 x 4 dva) of probe stimuli (gratings, 0.4 dva in diameter). Bottom: Drifting Gabor grating (1.5 dva in diameter) used for CRF stimulation, positioned within the joint receptive fields of recorded neurons. Zero (x, y) denotes the center of the CRF population. (D) Heatmap of visual responses from 159 neurons to 36 drift directions of Gabor gratings, vertically stacked along cortical depth (M1, *pen1*). Top: Distribution of differences in preferred orientation for all pairwise combinations of neurons.

geniculocortical inputs initially drive neurons within layers 4Cα and 4Cβ (Hubel and Wiesel, 1972; Hendrickson et al., 1978; Blasdel and Lund, 1983), which then propagate to supragranular and infragranular layers (Callaway, 1998; Callaway, 2004).

Nonclassical RF stimulation and border ownership

Within each of the recordings, we also examined the responses of V1 neurons to nCRF stimuli. It is known that neurons in primate visual cortex integrate visual information from far beyond their CRFs (Albright and Stoner, 2002; Allman et al., 1985; Fitzpatrick, 2000; Roelfsema, 2006; Angelucci et al., 2017). One example of contextual modulation is the selectivity of neurons to border ownership (B_{own}). Specifically, neurons in early visual areas respond differently to identical edges (borders) of objects when those objects lie at different locations outside the CRFs (Zhou et al., 2000; Franken and Reynolds, 2021; Hesse and Tsao, 2016; Hesse and Tsao, 2023) (**Figure 2**). As with other forms of nCRF modulation, B_{own} is thought to emerge either by feedback from higher areas (Craft et al., 2007; Jehee et al., 2007; Layton et al., 2012; Eguchi and Stringer, 2016; Wagatsuma et al., 2021; Mehrani and Tsotsos, 2021) or from horizontal connections within the same area (Zhaoping, 2005; Kogo et al., 2010). In V1, feedback and horizontal inputs arrive principally within supragranular and infragranular layers, i.e., they avoid layer 4 (Rockland and Pandya, 1979; Rockland and Lund, 1983; Rockland and Virga, 1989; Anderson and Martin, 2009; Markov et al., 2014; Federer et al., 2021; Gilbert and Wiesel, 1983; Shmuel et al., 2005; Siu et al., 2021). Thus, V1 activity generated by nCRF stimulation is known to involve different circuits compared to the activity generated by CRF stimulation.

In this study, border ownership test stimuli consisted of uniformly white or black objects (squares, 8 x 8 dva) on a black or white background, respectively, as in previous studies (Zhou et al., 2000) (Methods). One border of the object fell within the CRFs of the recorded neurons. Within the CRF, the oriented border could either be a dark-light edge or light-dark edge, resulting in two different local contrast polarity (LC) conditions (**Figure 2A**). Outside the CRF, the stimulus configuration differed for the same LC condition such that the oriented border could belong to opposite sides of an object relative to the CRF. Crucially, across these two object side conditions, the stimulus falling within the CRF was identical (**Figure 2B**) and was identical within an area that extended well beyond the CRF (8 x 16, dva). In this stimulus configuration, differences in evoked responses between the two object side conditions signify selectivity to border ownership (Zhou et al., 2000). The statistical significance was determined by a two-factor ANOVA on the mean spike counts for each condition, with object side (Side 1 and Side 2) and local contrast (LC1 and LC2) as the factors, along with their interaction (Methods).

We observed neurons with B_{own} in our recordings from macaque V1. **Figures 2C** and **2D** shows examples of four neurons selective to B_{own}. Each of these neurons exhibited a preference for LC, with two neurons preferring one contrast polarity and two preferring the other. In addition, each neuron responded differently depending on which side of the object appeared relative to the CRF, thus exhibiting B_{own}. Three of the neurons responded more vigorously to borders belonging to the lower-left side of object (Side 1) ($p < 10^{-14}$, 10^{-10}, 10^{-3} for neurons 1, 2, and 4, respectively), while one neuron responded more vigorously to the border belonging to the upper-right side of the object (Side 2) ($p = 0.014$, neuron 3). Furthermore, one of the neurons showed a consistent preference for Side 1 across both LCs (neuron 4).

To quantify the B_{own}, as in previous studies (Zhou et al., 2000), we calculated a B_{own} modulation index, defined as the difference in neuronal responses to borders belonging to opposite sides of objects, normalized by the maximum response for each neuron (Methods). Responses to the same side of object, but under opposite LC conditions, were averaged together to control for global luminance differences in the overall display. Across the 621 neurons recorded in four sessions, we found that 133 neurons (21.4% overall; *pen1* = 28.2%; *pen2* = 27.9%; *pen3* = 18.4%; *pen4* = 8.4%) responded differently to identical borders yet belonging to opposite sides of the object, a

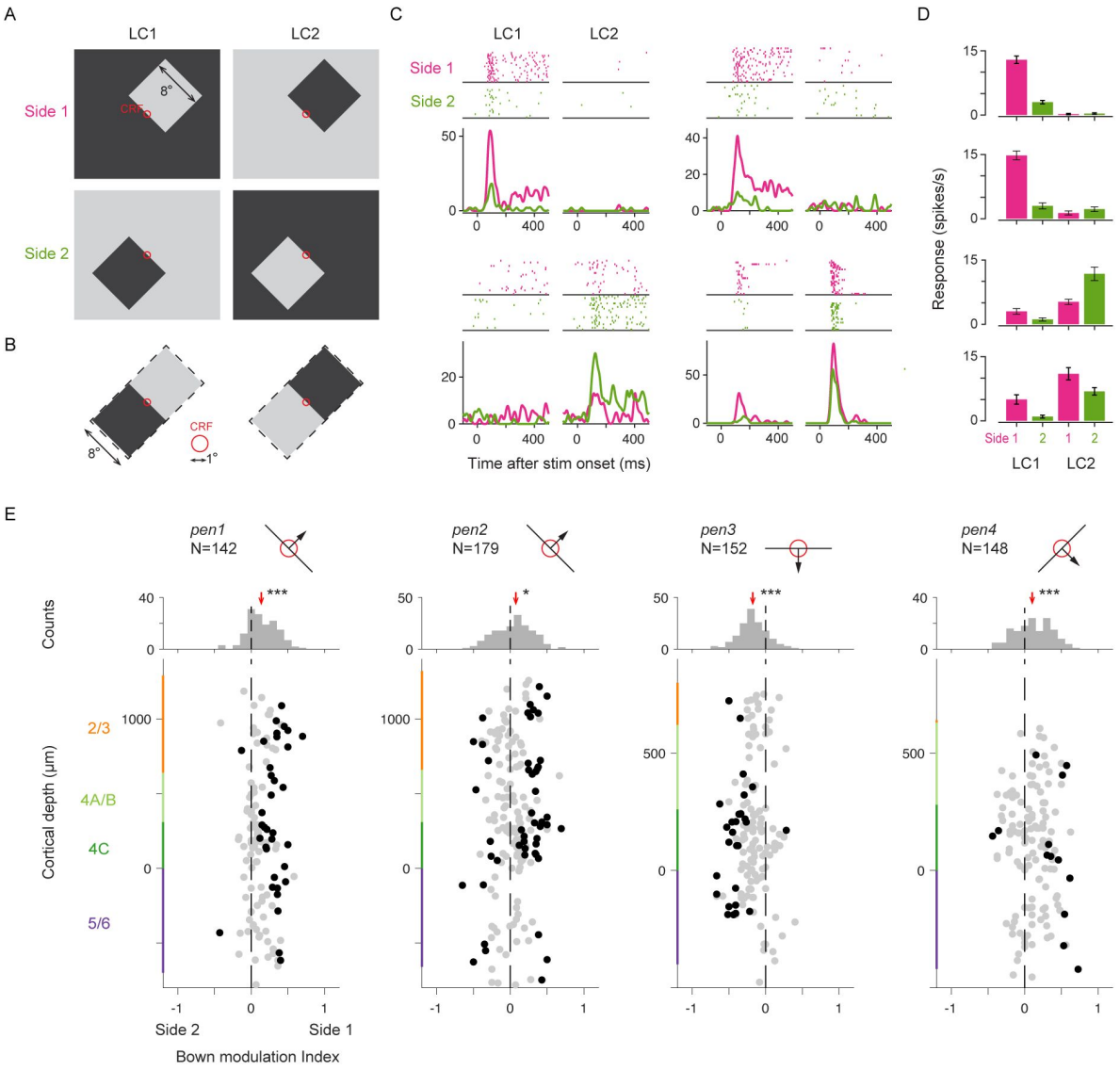

Figure 2.

Nonclassical receptive field (nCRF) stimulation and border ownership

(A) Border ownership test stimuli for nCRF stimulation. Stimuli consisted of uniformly white or black objects (8° squares) on black or white backgrounds, respectively. One border of the object fell within the CRFs (red circle) of the recorded neurons, with orientation varying in 45° steps. Within the CRF, depending on local contrast polarity (LC), the border could either be a dark-light edge (LC1, Left column) or a light-dark edge (LC2, Right column). For the same LC condition, the border within the CRF could be the bottom-left edge (Side 1, top row) or top-right edge (Side 2, bottom row) of the object. (B) Enlarged view of stimulus configuration within the CRF, showing identical stimulus regions between Side 1 and Side 2 for each LC condition (8 x 16 dva). (C) Four example B_{own} neurons recorded from V1. For each neuron, dot raster plots (top) and instantaneous firing rates (bottom) show responses to the four stimulus conditions depicted in (A), respectively. Magenta represents Side 1; green represents Side 2. (D) Bar plots showing the mean spike rates of the four neurons across the four stimulus conditions. (E) Top: Cartoon depicting the preferred border orientation for each of the four recording sessions (*pen*1-4). Arrows indicate the preferred side of objects relative to the border in the CRF. Bottom: B_{own} modulation index for each neuron plotted at its recorded cortical depth across the recordings. Color bars on the ordinate represent laminar compartments. Black dots denote statistically significant B_{own} neurons, determined by ANOVA with object side and local contrast as factors ($p < 0.05$). Middle: Marginal distribution of the B_{own} modulation index, red arrows indicating the population median. *$p < 0.05$; ***$p < 10^{-5}$.

proportion consistent with previous studies in awake monkeys (Zhou et al., 2000). Neurons with B_{own} were found within all cortical laminar compartments, including input layer 4C (5/6: 28/144 = 19.4%; 4C: 48/212 = 22.6%; 4A/B: 19/114 = 16.7%; 2/3: 28/99 = 28.3%) (**Table S1**), and the proportion was independent of laminar compartment ($\chi^2(3) = 4.78$, $p = 0.19$, chi-quare test of homogeneity). Of all V1 neurons, 96 (15.5%) exhibited B_{own} depending on the LC (5/6: 11.1%; 4C: 17.9%; 4A/B: 14.0%; 2/3: 20.2%), while 37 (6.0%) showed significant effects independent of local contrast (5/6: 8.3%; 4C: 4.7%; 4A/B: 2.6%; 2/3: 8.1%). Thus, the majority of V1 neurons with B_{own} exhibited selectivity for only one local contrast, and neurons with B_{own} invariant to local contrast were rare, also consistent with previous observations (Zhou et al., 2000).

Columnar organization of border ownership selectivity

We next considered whether neurons with B_{own} comprised a distinct group, or instead reflected a general tendency of neurons to prefer one side of the object, with statistically significant neurons falling at the tails of the distribution. We leveraged the large number of simultaneously recorded single neurons to measure the distribution of B_{own} modulation across laminar compartments in each session. We found that in each of the four recordings, the distributions of B_{own} modulation generally appeared unimodal, with neurons exhibiting B_{own} falling at the distribution tails (**Figure 2E**). Surprisingly, we also found that within individual recordings, neurons across the cortical depth tended to share similar preferences for the side of the object. That is, for each recording, the B_{own} modulation index differed significantly from 0 (Median modulation index: *pen1* = 0.14, $p < 10^{-12}$; *pen2* = 0.08, $p = 0.04$; *pen3* = −0.18, $p < 10^{-15}$; *pen4* = 0.10, $p < 10^{-5}$, sign test against zero-median). For example, the first recording (*pen1*) was performed in a column in which most neurons preferred an orientation of 135°. In addition, within that column, neurons tended to exhibit higher responses to a border when it belonged to the lower-left side of an object (side 1), as opposed to the upper-right side (side 2). Thus, V1 exhibited a continuum of B_{own}, and neurons within single columns tended to prefer the same side of objects located outside of the CRF.

Interlaminar cross-correlations among neurons within single V1 columns

The large number of simultaneously recorded neurons from each session also allowed us to measure interlaminar information flow among single neurons under different visual stimulation conditions. Temporally precise cross-correlations in spike trains offer a unique means of assessing functional interactions among neurons in neural circuits (Perkel et al., 1967). Cross-correlations can be interpreted as suggesting one of myriad putative circuit arrangements among neuronal ensembles (Moore et al., 1970; Aertsen and Gerstein, 1985; Melssen and Epping, 1987; Ostojic et al., 2009). The identification of such interactions has played an important role in elucidating neural circuits in the mammalian visual system (Ts'o et al., 1986; Schwarz and Bolz, 1991; Reid and Alonso, 1995; Alonso et al., 1996; Alonso and Martinez, 1998; Usrey et al., 1998; Nelson et al., 1992; Briggs et al., 2013; Roe and Ts'o, 1999; Senzai et al., 2019; Denman and Contreras, 2014; Siegle et al., 2021; Jia et al., 2022; Trepka et al., 2022; Smith and Kohn, 2008; Sibille et al., 2022). In particular, it has been useful in specifying the flow of signals through local neural circuits (Trepka et al., 2022) and distributed networks (Siegle et al., 2021; Jia et al., 2022; Sibille et al., 2022). Notably, past studies have demonstrated that neuronal cross-correlations are dynamic and can depend on stimulus context and behavioral variables (Hembrook-Short et al., 2019; Martin and von der Heydt, 2015; Hung et al., 2007; Hirabayashi and Miyashita, 2005; Hirabayashi et al., 2010; Steinmetz et al., 2000).

Given that V1 activity generated by nCRF stimulation is thought to involve different circuitry than activity generated by CRF stimulation (Angelucci et al., 2017), we next asked if the pattern of cross-correlations measured under classical and nonclassical stimulus conditions might differ in a manner consistent with models of their underlying circuitry. Specifically, modulation of visual responses during nCRF stimulation, such as border ownership stimuli, is thought to emerge from either feedback from higher areas or horizontal connections within the same areas (Bair et al.,

2003; Bullier et al., 2001; Hupe et al., 1998; Chen et al., 2017; Gieselmann and Thiele, 2022; Keller et al., 2020; Klink et al., 2017; Nassi et al., 2013; Nurminen et al., 2018; Angelucci et al., 2017; Angelucci and Bressloff, 2006; Ichida et al., 2007; Schwabe et al., 2006; Pak et al., 2020; Vangeneugden et al., 2019; Zhang et al., 2014; Adesnik et al., 2012; Chisum et al., 2003; Stettler et al., 2002; Liang et al., 2017; Craft et al., 2007; Jehee et al., 2007; Chen et al., 2014; Self et al., 2013; van Kerkoerle et al., 2014), both arriving principally in superficial (layers 1-3) and deep (layers 5-6) layers (Rockland and Lund, 1983; Rockland and Pandya, 1979; Rockland and Virga, 1989; Markov et al., 2014; Federer et al., 2021; Anderson and Martin, 2009; Gilbert and Wiesel, 1983; Shmuel et al., 2005; Siu et al., 2021). In contrast, CRF responses are driven predominantly by feedforward circuitry and geniculocortical inputs to layers 4C (Hubel and Wiesel, 1972; Hendrickson et al., 1978; Blasdel and Lund, 1983; Callaway, 1998; Callaway, 2004). This suggests that the pattern of cross-correlations among neurons across V1 layers may differ under CRF and nCRF stimulus conditions.

Across recording sessions, we calculated cross-correlograms (CCGs) from all possible pairwise combinations of neuronal spike trains during both CRF (Gabor gratings) and nCRF (border ownership) stimulation conditions. **Figure 3A** shows an example recording session (M1, *pen1*) in which 159 visually responsive neurons were recorded during CRF stimulation, and CCGs were computed for 7,956 pairwise combinations of neurons (Methods). CCGs were determined to be significant if the jitter-corrected CCG peak occurred within 10ms of zero-time lag, and exceeded 7 standard deviations (SD) above the mean of the noise distribution (Siegle et al., 2021; Trepka et al., 2022) (Methods). In this recording, 13.8% of the total CCGs computed were found to be significant. Eight significant pairs are highlighted in **Figure 3A**, with their corresponding CCGs shown in **Figure 3B**. The peak lag (PL), defined as the relative time delay in occurrence of peak correlation between two spike trains, was restricted to within 10ms. This metric approximates the synchrony and/or the direction of information flow between neuronal pairs (Aertsen and Gerstein, 1985; Moore et al., 1970; Melssen and Epping, 1987; Ostojic et al., 2009). These examples illustrate the tendency of CCGs to corroborate the circuitry within V1 columns under CRF conditions in that 1) PLs generally increase with larger distances between pairs, and 2) layer 4 neurons tend to lead superficial neurons (Trepka et al., 2022). We exploited this latter point to test the extent to which the sequence of information flow across layers differs between CRF and nCRF conditions.

Comparison of cross-correlations during CRF and nCRF stimulation

From the 677 and 621 neurons recorded across the 4 recording sessions during CRF and nCRF stimulation, there were 41,759 and 28,430 pairwise combinations included, respectively (Methods). Of those, we found that 6,937 (16.6%) and 4,826 (17.0%) of the CCGs were significant (CRF: *pen1*: 1099/7956 = 13.8%, *pen2*: 2402/11431 = 21.0%, *pen3*: 2174/17780 = 12.2%, *pen4*: 1262/4592 = 27.5%; nCRF: *pen1*: 447/2473 = 18.1%, *pen2*: 2750/11823 = 23.3%, *pen3*: 839/6998 = 12.0%, *pen4*: 790/7136 = 11.1%). Notably, the proportion of significant connections were nearly identical under the two stimulus conditions, and also were within the range observed in previous studies of macaque V1 (Chu et al., 2014; Hembrook-Short et al., 2019; Smith and Kohn, 2008; Kohn and Smith, 2005).

As noted above, modulation of visual responses during nCRF stimulation, such as border ownership stimuli, is thought to be generated principally by feedback/horizontal connections arriving within superficial and deep layers, which contrasts with feedforward input driving CRF stimulation (**Figure 3C**). Thus, we asked whether cross-correlations between pairs of neurons situated across laminar compartments depended on the type of visual stimulation. We focused our analysis on CCGs computed from pairs of neurons in which one neuron was located within laminar compartments receiving feedback/horizontal inputs (FH_i), namely layers 2/3 and 5/6, and the other was located within compartments relatively devoid of those inputs, namely 4C and 4A/B.

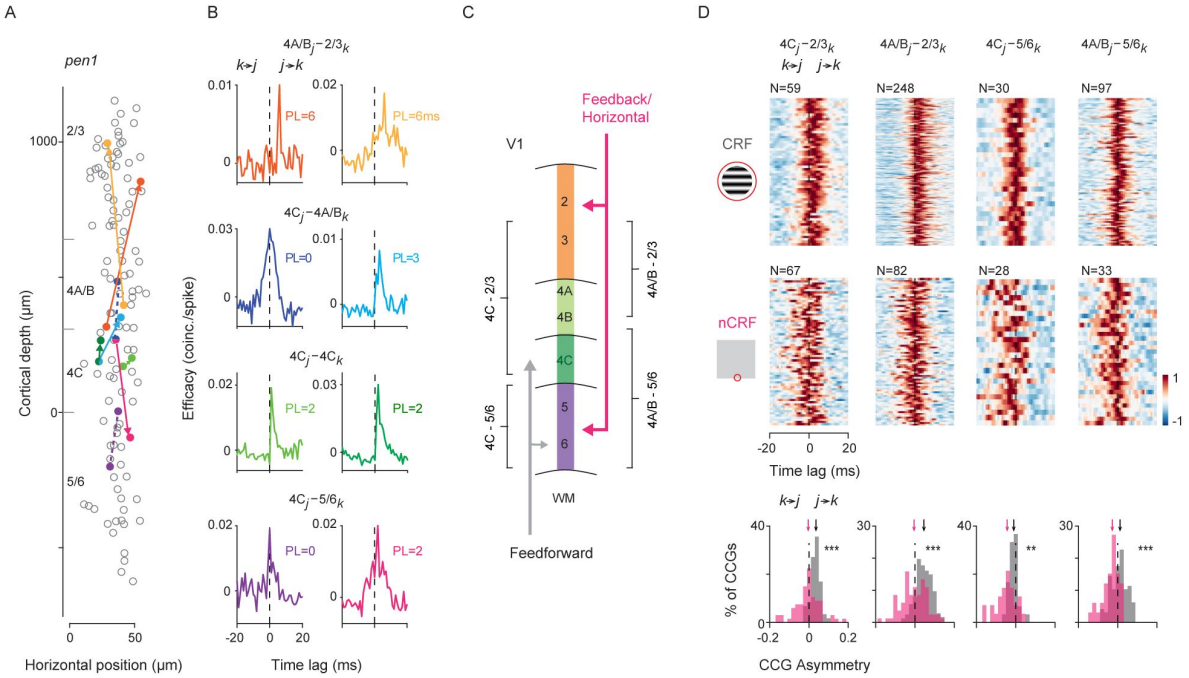

Figure 3.

Interlaminar cross-correlations during CRF and nCRF stimulation

(A) Example recording (M1, *pen1*) showing 159 visually responsive neurons (circles) recorded simultaneously during CRF stimulation, plotted at their relative cortical depth. The abscissa is magnified for visualization. Also shown are eight example neuronal pairs with significant CCGs during CRF stimulation. Neuronal pairs with zero-time lag CCGs are connected by dashed lines, while pairs with nonzero-time lag CCGs are connected by arrowed lines, with the arrow pointing to the lagging neuron. (B) Eight corresponding CCGs from (A). Neuronal pairs are separated by their laminar compartment combinations. The reference neuron (1st neuron in the CCG function) is designated as *j*, and the target neuron as *k*. PL (peak lag, ms) is defined as the relative time delay in peak correlation between the two spike trains. (C) Diagram illustrating feedforward and feedback (and horizontal) projections within the designated laminar compartments. Feedforward inputs arrive within laminar compartments 4C, while feedback (and horizontal) projections principally target superficial and deep layers. (D) Heatmap of all significant CCGs during either CRF stimulation (Gabor gratings, top row) or nCRF stimulation (border ownership, middle row), for the four key interlaminar combinations (columns), calculated from one example recording (M1, *pen1*). Individual CCGs are normalized by their absolute maximum for visualization, and different CCGs are vertically stacked. Bottom row: Distribution of CCG asymmetry for each of the four key interlaminar compartments as in (A), across CRF stimulation (gray) and nCRF stimulation (magenta). Arrows indicate the population median. **$p < 0.002$; ***$p < 10^{-5}$.

This analysis compared the relative spike timing between neuronal pairs during CRF and nCRF stimulation. If indeed FH_i contribute more to activity during the latter than the former, then we should expect this to be reflected in lead-lag relationships of the CCGs.

A comparison of V1 CCGs from key interlaminar neuronal pairs during CRF and nCRF stimulation is shown for an example recording session (M1, *pen1*) in **Figure 3D**. During CRF stimulation, the timing of spikes within compartments 4C and 4A/B generally preceded, or was simultaneous with, spikes within FH_i compartments (CRF: 4C-2/3_{PL} = 2ms, $p < 10^{-7}$; 4A/B-2/3_{PL} = 2ms, $p < 10^{-28}$; 4C-5/6_{PL} = 0ms, p = 0.52; 4A/B-5/6_{PL} = 0ms, p = 0.64; Sign test against zero-median). In contrast, during nCRF stimulation, relative spike timing was shifted in favor of neurons in FH_i compartments. Specifically, during nCRF stimulation, the timing of spikes within compartments 4C and 4A/B lagged or was simultaneous with, spikes within FH_i compartments (nCRF: 4C-2/3_{PL} = 0ms, p = 0.80; 4A/B-2/3_{PL} = 0ms, p = 0.70; 4C-5/6_{PL} = −2.5ms, p = 0.11; 4A/B-5/6_{PL} = 0ms, p = 0.56; Sign test against zero median). To further quantify the apparent shift in lead-lag relationships, we calculated an asymmetry index for each CCG. The asymmetry index is computed as the difference in the CCG integral on either side of zero-time lag, and summarizes the lead-lag relationship independent of the CCG peak (Jia et al., 2022) (Methods). Consistent with the analyses of PL, we found that CCG asymmetries differed significantly between CRF and nCRF stimulation for each of the interlaminar comparisons. In each case, the distribution of asymmetries during nCRF stimulation shifted to favor neurons in FH_i laminar compartments, when compared to CRF stimulation (4C-2/3: CRF_{Asym} = 0.036, $nCRF_{Asym}$ = −0.004, Δ = −0.04, $p < 10^{-6}$; 4A/B-2/3: CRF_{Asym} = 0.046, $nCRF_{Asym}$ = −0.005, Δ = −0.051, $p < 10^{-11}$; 4C-5/6: CRF_{Asym} = −0.010, $nCRF_{Asym}$= −0.044, Δ = −0.034, p = 0.0015; 4A/B-5/6: CRF_{Asym} = 0.012, $nCRF_{Asym}$ = −0.028, Δ = −0.04, $p < 10^{-5}$; Wilcoxon rank-sum test). Thus, CCG data from this single recording session indicated that relative spike timing was earlier within FH_i laminar compartments during nCRF stimulation than during CRF stimulation.

Across all recordings, we identified a total of 2,573 and 2,118 significant neuronal pairs from the four interlaminar combinations during CRF (*pen1* = 274; *pen2* = 1187; *pen3* = 560; *pen4* = 302) or nCRF stimulation (*pen1* = 210; *pen2* = 1226; *pen3* = 382; *pen4* = 300), respectively, and compared their CCG asymmetries. Similar to the pattern observed in the example recording, we observed a consistent shift in lead-lag relationships for each of the interlaminar comparisons (**Figure 4**). Specifically, during nCRF stimulation, the distribution of asymmetries during nCRF stimulation shifted to favor neurons in FH_i laminar compartments, when compared to CRF stimulation (4C-2/3: CRF_{Asym} = 0.028, $nCRF_{Asym}$ = 0.012, Δ = −0.016, $p < 10^{-9}$; 4A/B-2/3: CRF_{Asym} = 0.038, $nCRF_{Asym}$ = 0.022, Δ = −0.016, $p < 10^{-9}$; 4C-5/6: CRF_{Asym} = −0.033, $nCRF_{Asym}$ = −0.047, Δ = −0.014, $p < 10^{-5}$; 4A/B-5/6: CRF_{Asym} = −0.018, $nCRF_{Asym}$ = −0.05, Δ = −0.032, $p < 10^{-20}$; Wilcoxon rank-sum test). Thus, relative spike timing was earlier within FH_i laminar compartments during nCRF stimulation than during CRF stimulation in the combined dataset, suggesting that the proportion of information flow from FH_i layers to input layers increased during nCRF stimulation. This observation was consistent across individual recording sessions (**Table S2**). Notably, we observed a similar pattern when instead of asymmetry, we compared CCG peak lags (**Supplementary Figure S2A**), and when we compared the total number of both significant and nonsignificant pairs (CRF = 15,920; nCRF = 11,263) (**Supplementary Figure S2B**), and when we compared CCGs with a more stringent significance criterion (10 SDs) in the combined dataset (**Supplementary Figure S2C-D**).

Lastly, we asked whether interlaminar information flow was related specifically to border ownership modulation, independent of the comparisons between CRF and nCRF stimulation. Since CRF and nCRF stimuli differed in ways potentially unrelated to nonclassical modulation (e.g., variations within the CRF), we sought to assess the extent to which information flow from FH_i to input layers predicted the magnitude of nCRF modulation. To this end, we computed two modulation indices from the same B_{own} test stimuli (**Figure 2A**), specifically the B_{own} modulation index and the local contrast (LC) index. In contrast to the B_{own} modulation index, which reflects nCRF modulation, the LC index measures selectivity to luminance contrast polarity

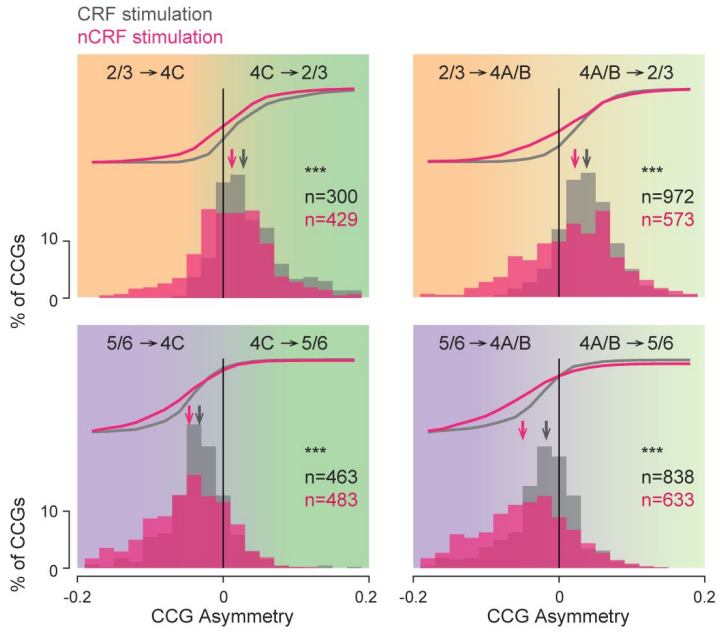

Figure 4.

Comparison of interlaminar CCG asymmetries during CRF and nCRF stimulation

Combined dataset for each of the four key interlaminar combinations. Histograms and cumulative distributions of asymmetry for all significant CCGs during CRF (gray) and nCRF (magenta) stimulation. Arrows indicate the population median. ***$p < 10^{-5}$.

(dark-light vs. light-dark) within the CRF. We hypothesized that if the relative timing of spiking activity within FH_i laminar compartments is indicative of nCRF modulation, we should expect earlier relative spike timing in FH_i compartments, i.e., lower CCG asymmetries with respect to other compartments, to be associated with greater B_{own}. In contrast, we should not expect that relationship with the LC index.

Consistent with our hypothesis, we observed a negative relationship between the B_{own} modulation index and CCG asymmetry across the population and within individual sessions (linear regression: population slope (β) = −0.32, $p < 10^{-27}$; individual sessions: *pen1* = −0.52, $p < 10^{-5}$; *pen2* = −0.06, p = 0.14; *pen3* = −0.25, $p < 10^{-4}$; *pen4* = −0.20, p = 0.008) (**Figure 5A**). This result suggests that the magnitude of B_{own} modulation for neuronal pairs depended on the proportion of information flow from FH_i compartment to input layers. In contrast, the opposite was true for the LC index. That is, LC index was positively correlated with CCG asymmetry across the population (linear regression: population slope (β) = 0.46, $p<10^{-28}$) (**Figure 5B**). However, this relationship was not consistent across sessions (individual sessions: *pen1* = −0.30, p = 0.09; *pen2* = 0.33, $p < 10^{-5}$; *pen3* = 0.23, p = 0.006; *pen4* = 0.14, p = 0.04). To explore both results further, we built generalized linear models (GLMs) to assess the dependence of B_{own} or LC modulation on CCG asymmetry to incorporate variations across interlaminar combinations and recording sessions. For LC modulation, this analysis indicated that the magnitude of LC modulation was not reliably predicted by interlaminar information flow (GLM: coefficient = −0.04, p = 0.30; $R^2 = 0.27$) (**Table S3**). In contrast, for B_{own} modulation, this analysis confirmed that the magnitude of modulation was reliably predicted by interlaminar information flow, independent of variations across interlaminar combinations and recording sessions (GLM: coefficient = −0.16 $p = 1.1*10^{-6}$; $R^2 = 0.11$). These results demonstrate that interlaminar information flow was related specifically to the magnitude of border ownership modulation.

Discussion

We measured the sensitivity of neurons to nCRF stimulation, specifically border ownership, within large, local populations in macaque V1. Consistent with previous studies on awake animals, we observed V1 neurons with border ownership selectivity even under anesthesia. We observed that neurons within single columns tended to prefer the same side of objects located outside of the CRF. In addition, we found that cross-correlations among pairs of neurons situated across FH_i and other laminar compartments differed between CRF and nCRF stimulation. Specifically, neurons within FH_i laminar compartments were more likely to lead pairwise interactions with neurons in other compartments during nCRF stimulation than during CRF stimulation. Moreover, the magnitude of border ownership modulation was predicted by greater information flow from FH_i laminar compartments, independent of the comparisons between CRF and nCRF stimulation. These results demonstrate that the flow of signals between neurons in FH_i and other laminar compartments depends on the degree to which those neurons integrate visual information from beyond the CRF. Below we discuss some potential limitations of the results as well as their implications for the mechanisms underlying contextual modulation.

The observation that neurons within FH_i laminar compartments can lead those in layer 4 during nCRF stimulation may appear surprising. However, several anatomical pathways could mediate the propagation of B_{own} signals from FH_i compartments to layer 4. In macaque V1, layers 5/6 send dense projections to 4A/B (Lund, 1988; Callaway, 1998). In particular, layer 6 pyramidal neurons, especially the subset classified as Type 1 cells, project substantially to layer 4C (Wiser and Callaway, 1996; Fitzpatrick et al., 1985). Projections from layers 2/3 to 4A/B have also been reported (Blasdel et al., 1985; Callaway and Wiser, 1996), and neurons in 4A/B often extend apical dendrites into layers 2/3 (Lund, 1988; Yoshioka et al., 1994). Although direct projections from layers 2/3 to 4C are generally sparse (Callaway, 1998), a subset of neurons in the lower part of layer 3 can give off collateral axons to 4C (Lund and Yoshioka, 1991). Additionally, some 4C

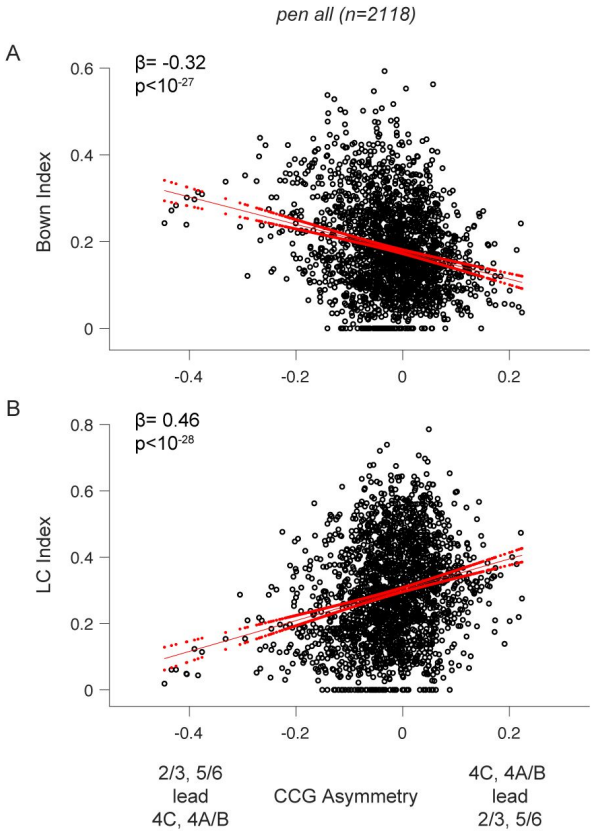

Figure 5.

Dependence of nCRF modulation on interlaminar signal flow

(A) Scatter plot of the B_{own} modulation index versus CCG asymmetry for all significant CCGs, aggregated across the four key interlaminar combinations and all recording sessions. CCG asymmetries were calculated during nCRF stimulation. The geometric mean of the B_{own} index for each neuronal pair was used. Red lines denote the fitted regression line and the 95% confidence interval in linear regression. (B) Similar to (A), but using the local contrast (LC) index instead of the B_{own} index. The LC index was calculated as the difference in neuronal responses to borders with opposite contrast polarities, normalized by the maximum response.

neurons extend dendrites into 4B, enabling potential dendritic integration of inputs from more superficial layers (Somogyi and Cowey, 1981; Mates and Lund, 1983; Yabuta and Callaway, 1998). Moreover, layers 2/3 may influence 4C neurons disynaptically, without requiring dense monosynaptic connections. Importantly, while CCGs can suggest possible circuit arrangements, functional connectivity may arise through mechanisms not fully captured by traditional anatomical tracing. Our observation of functional inputs from layers 2/3 to layer 4 aligns with prior findings in rodent V1, where CCG analysis (Senzai et al., 2019) or photostimulation (Xu et al., 2016) revealed similar pathways. Nonetheless, future studies will be needed to determine the extent of input to layer 4 neurons from more precise FHi laminae.

Each of the laminar compartments designated in this study comprised more than a single distinct anatomical layer. This was done to mitigate the uncertainty in determining exact laminar boundaries, to achieve comparable numbers of neurons across compartments, and to maximize statistical power. In addition, combining layers allowed us to combine feedback with horizontal input layers. It is known that feedback and horizontal connections exhibit layer specificity within superficial and deep layers, e.g., horizontal connections are most prominent in layer 2/3 and 5 (Rockland and Lund, 1983; Gilbert and Wiesel, 1983), where feedback connections target primarily in layers 1, upper layer 2, and 5/6 (Rockland and Pandya, 1979; Federer et al., 2021; Shmuel et al., 2005). Yet, they both largely avoid layer 4 (Angelucci et al., 2017). Nonetheless, given that the number of anatomically distinct layers within macaque V1 well exceeds the four designated laminar compartments used here, it is important to consider the extent to which collapsing layers limits the conclusions one can draw from our observations. For example, although layer 6 receives feedback input, it also receives feedforward input directly from the LGN (Hubel and Wiesel, 1972; Hendrickson et al., 1978; Blasdel and Lund, 1983; Callaway, 1998). In addition, layer 4A is generally considered an input layer whereas 4B is not (Callaway, 1998; Hubel and Wiesel, 1972; Blasdel and Lund, 1983; Hendrickson et al., 1978). Thus, the designation of any compartment as nominally input, or feedback was relative and not absolute. That is, superficial (layers 2/3) and deep (layers 5/6) layers receive higher proportions of feedback/horizontal inputs than the 4A/B and 4C compartments. Indeed, previous studies of primate visual cortex have used a similar approach in comparing input and feedback/horizontal laminar compartments (e.g. Hansen et al., 2012; Nandy et al., 2017; van Kerkoerle et al., 2017; Pettine et al., 2019). Thus, the observed changes in pattern of cross-correlations between neurons situated across compartments with different relative feedforward and feedback/horizontal input can be interpreted in light of those input differences.

Another important consideration is that a key challenge of studying classical and nonclassical RF effects simultaneously in large neuronal populations is the difficulty in achieving alignment of all CRFs with the test stimuli. Although our probe penetrations were largely normal to the surface and neurons showed minimal deviations in orientation selectivity across the cortical depth, V1 neurons nonetheless exhibit noteworthy RF scatter (location/size) even within single cortical columns (Tootell et al., 1988; Gur et al., 2005; Li et al., 2022). This means that the positioning of stimuli relative to the CRF inevitably varied across simultaneously recorded neurons (e.g., **Figure 1C**). Moreover, this means that although neurons were generally well driven by CRF grating stimuli and exhibited clear orientation tuning, CRF stimulation was not guaranteed to fall solely within the CRF of all neurons. Nonetheless, involvement of the surround, especially far surround was considerably less extensive for CRF stimulation than for nCRF stimulation. Furthermore, in the latter case, regardless of variability in the CRF location, stimuli falling within the CRF were always matched across nCRF stimulus conditions, and the surrounds were also identical within 8° of the CRF (**Figure 2A, B**).

The experiments described here were performed in anesthetized animals. Several other types of contextual modulation have been demonstrated in anesthetized animals (Ramsden et al., 2001; Hupe et al., 1998; Bair et al., 2003; Allman et al., 1985; Gilbert and Wiesel, 1990; Nothdurft et al., 1999; Webb et al., 2003; Zarella and Ts'o, 2016; Muller et al., 2003; Henry et al.,

2013; Bijanzadeh et al., 2018), and can involve inter-cortical feedback (Nurminen et al., 2018). Nonetheless, anesthesia is known to affect certain types of contextual responses in area V1. For example, the "figure-ground segregation" effect, where neurons respond more strongly to a texture in a "figure" region than to the same texture in a "ground" region, has been shown to be suppressed under anesthesia (Lamme et al., 1998) and when figure stimuli are not perceived (Super et al., 2001). However, there has been debate over whether this effect depends on attention and awareness (Marcus and Van Essen, 2002; Jones et al., 2015; Poltoratski and Tong, 2020; Poort et al., 2012; Huang et al., 2020). It is worth noting that in that case, RFs are centered on the figure regions, and the modulation likely involves detecting feature discontinuities around boundaries, followed by region-filling and background suppression. Each step could be influenced differently by behavioral variables. Nevertheless, the center figure enhancement emerges late in the V1 response, ~55ms after response onset (Poort et al., 2012). In contrast, border ownership involves RFs centered on the boundaries, with modulation emerging much earlier at ~10-35ms after response onset (Sugihara et al., 2011). Therefore, although both forms of modulation may involve feedback/horizontal input, the underlying circuitry may differ. Our finding of border ownership modulation in anesthetized animals aligns with previous studies showing that border ownership modulation can act separately even without attention (Qiu et al., 2007; O'Herron and von der Heydt, 2009) or before object shape recognition (Williford and von der Heydt, 2016; Ko and von der Heydt, 2018), perhaps signifying a representation of "proto-objects" in the early visual cortex through automatic, pre-attentive grouping mechanism (von der Heydt, 2015; von der Heydt, 2023; Self et al., 2019).

Border ownership enables neurons with small CRFs in the early visual cortex to assign the occluding border between image regions to a foreground object, which is crucial for natural scene segmentation and object recognition (Nakayama et al., 1995). Human imaging studies have demonstrated the existence of B_{own} in both lower (Fang et al., 2009) and higher visual areas (Kourtzi and Kanwisher, 2001; Andrews et al., 2002), yet the underlying circuitry is still poorly understood. Several computational models have been proposed to explain B_{own}, including feedforward models (Walker et al., 1999; Sakai and Nishimura, 2006; Super et al., 2010), horizontal models (Zhaoping, 2005; Kogo et al., 2010), and feedback models (Craft et al., 2007; Jehee et al., 2007; Jeurissen et al., 2016). Yet cues for determining B_{own} often lie far from the CRF and beyond the extents of geniculocortical and horizontal V1 connections (Angelucci et al., 2017). Furthermore, conduction along horizontal fibers appears too slow (0.1-0.4 mm/ms) (Grinvald et al., 1994; Bringuier et al., 1999; Girard et al., 2001) to account for the rapid (~10-35ms) emergence of B_{own} and its independence from object size (Zhang and von der Heydt, 2010; Sugihara et al., 2011). In contrast, feedback inputs can be conducted through fibers 10 times faster (20-60 mm/ms) (Girard et al., 2001), even via monosynaptic connections (Siu et al., 2021), and contribute to modulating the early responses of V1 neurons (Hupe et al., 2001; Bair et al., 2003). Thus, although we combined feedback and horizontal recipient layers, the differences in interlaminar signal flow we observed were likely driven predominantly by feedback inputs.

In primates, V1 receives inter-cortical feedback connections primarily from areas V2, V3, V4, MT (Rockland et al., 1994; Markov et al., 2014). Thus, V1 B_{own} signals could be generated via inputs from these areas (Zhou et al., 2000; Hesse and Tsao, 2016; Hesse and Tsao, 2023; Franken and Reynolds, 2021; Zhu et al., 2020). Our results resonate with a recent study reporting that in area V4, B_{own} emerges earliest in deep layers compared to input layers (Franken and Reynolds, 2021). This suggests that the earliest component of B_{own} in V4 is not inherited from feedforward inputs, i.e., from V1/V2, but is generated within deep layers de nova, or through feedback connections that arrive at deep layers (Franken and Reynolds, 2021). This further supports the view that B_{own} in V1 emerges via feedback from higher visual areas. In addition, similar to what we observed in V1, columnar organization of B_{own} was observed in V4 (Franken and Reynolds, 2021). Indeed, neurons with B_{own} are clustered into patches in a wide range of primate visual areas, including area V2, V3, V3A, V4, V4A (Hesse and Tsao, 2023). Thus, the

evidence of B_{own} modularity we observed in V1 could arise from organized feedback from the B_{own} modules in those areas. This is supported by recent anatomical evidence suggesting that feedback terminals in V1 are clustered and functionally specific (Angelucci et al., 2002; Federer et al., 2021; Shmuel et al., 2005; Siu et al., 2021).

Methods

Experimental Model and Subject Details

Anesthetized recordings were conducted in two adult male rhesus macaques (*Macaca mulatta*, M1, 13 kg; M2, 8 kg). All experimental procedures were in accordance with the National Institutes of Health Guide for the Care and Use of Laboratory Animals, the Society for Neuroscience Guidelines and Policies, and with approved Institutional Animal Care and Use Committee (IACUC) protocol (#APLAC-9900) of Stanford University.

Electrophysiological Recordings

Prior to each recording session, treatment with dexamethasone phosphate (2 mg per 24 h) was instituted 24 h to reduce cerebral edema. After administration of ketamine HCl (10 mg per kilogram body weight, intramuscularly), monkeys were ventilated with 1-2% isoflurane in a 1:1 mixture of N_2O and O_2 to maintain general anesthesia. Electrocardiogram, respiratory rate, body temperature, blood oxygenation, end-tidal CO_2, urine output and inspired/expired concentrations of anesthetic gasses were monitored continuously. Normal saline was given intravenously at a variable rate to maintain adequate urine output. After a cycloplegic agent (atropine sulfate, 1%) was administered, the eyes were focused with contact lenses on an LCD monitor. Vecuronium bromide (60 μg/kg/h) was infused to prevent eye movements.

With the anesthetized monkey in the stereotaxic frame, an occipital craniotomy was performed over the opercular surface of V1. The dura was reflected to expose a small (~3 mm^2) patch of cortex. Next, a region relatively devoid of large surface vessels was selected for implantation, and the Neuropixels probe was inserted with the aid of a surgical microscope. Given the width of the probe (70 μm x 20 μm), insertion of it into the cortex sometimes required multiple attempts if it flexed upon contacting the pia. The junction of the probe tip and the pia could be visualized via the (Zeiss) surgical scope, and the relaxation of pia dimpling was used to indicate penetration, after which the probe was lowered at least 3-4 mm. Prior to probe insertion, it was dipped in a solution of the DiI derivative FM1-43FX (Molecular Probes, Inc) for subsequent histological visualization of the electrode track.

Given the length of the probe (1 cm), and the complete distribution of electrode contacts throughout its length, recordings could be made either in the opercular surface cortex (M1, *pen* 1-2) or within the underlying calcarine sulcus (M2, *pen* 3-4), by selecting a subset of contiguous active contacts (n = 384) from the total number (n=986). Recordings were made at 1 to 2 sites in one hemisphere of each monkey. At the end of the experiment, monkeys were euthanized with pentobarbital (150 mg/kg) and perfused with normal saline followed by 1 liter of 1% (wt/vol) paraformaldehyde in 0.1 M phosphate buffer, pH 7.4.

Visual Stimulation

Visual stimuli were presented at manually mapped receptive field (RF) locations for each recording session on an LCD monitor (Model NEC-4010, dimensions: 88.5 cm (H) x 49.7 cm (V), resolution: 1360 x 768 pixels, frame rate: 60 Hz) positioned 114 cm from the monkeys. RF eccentricities were ~4-6° (M1) and ~6-10° (M2). Visual stimuli were generated using customized MATLAB scripts with the Psychophysics Toolbox extensions (version PTB-3) (Kleiner et al., 2007). A photodiode was used to measure stimulus timing.

Classical receptive field (CRF) stimuli consisted of drifting Gabor gratings (2 deg./sec., 100% Michelson contrast) with a diameter of 1.5 degrees of visual angle (dva), positioned within the joint receptive fields (RFs) of recorded neurons. This size was selected to largely constrain the stimuli within the CRFs of recorded neurons, typically ~0.5-1 dva, as determined manually online. Gratings drifted in 36 different directions, from 0 to 360° in 10° steps, in a pseudorandom order. Each stimulus condition was presented for 1 s and repeated 5 or 10 times. A blank screen with equal luminance to the Gabor patch was presented for 0.25 s during the stimulus interval. Stimuli were presented either monocularly (*pen* 1, 3) or both monocularly and binocularly (*pen* 2, 4). Four spatial frequencies (0.5, 1, 2, 4 cycles/deg.) were tested. The optimal eye and spatial frequency conditions were determined offline for further analysis.

Nonclassical receptive field (nCRF) stimuli used in this study, i.e., Border ownership test stimuli consisted of uniformly white or black objects (square, 8 x 8 dva) presented on a black or white background, respectively, like previous studies (Zhou et al., 2000). One border of the object fell within the CRFs of the recorded neurons at an orientation that varied in 45° steps. Objects were either 4 x 4 dva or 8 x 8 dva in size, and only conditions with 8 x 8 dva were selected for quantifying border ownership selectivity to tolerate the variation in the CRF locations. Stimuli were presented monocularly to the preferred eye, to avoid the surround stimulating the CRF of the non-preferred eye. For each of the 4 orientation conditions, there were 4 basic conditions (**Figure 2A**). Within the CRF, the oriented border could either be a dark-light edge or light-dark edge, resulting in two different local contrast (LC) polarity conditions, namely, LC1 and LC2. For the same LC condition, the stimulus configuration outside of the CRF differed such that the oriented border could belong opposite sides of objects, resulting in two different sides of object conditions, namely, side 1 and side 2. Each stimulus condition was presented for 1 s and repeated 10 or 20 times. A blank screen with equal luminance to the mean of object and background luminance was presented for 0.5s during the stimulus interval.

Receptive field mapping

In some sessions, the receptive fields of V1 neurons were tested systemically for offline use. CRFs were mapped from a 10 x 10 array (4 x 4 dva) using probe stimuli. The array was centered at the manually determined RFs location. The stimuli consisted of circular sine wave gratings of 0.4 dva in diameter, and 100% Michelson contrast. Gratings were presented at the optimal orientation determined manually online for each recording session and drifted at speed of 2 deg./sec. Each stimulus condition was presented for 0.2s, interleaved with 0.3s of blank screen with equal luminance, and repeated 15 times.

Mean spike counts from 0.05 to 0.25s after each stimulus onset were calculated, resulting in a 10 x 10 matrix containing mean spike rates to each grid location. This 2D matrix was then interpolated to a 40 x 40 matrix (MATLAB function 'interp2') and then smoothed with a 2D Gaussian filter (MATLAB function 'imgaussfilt', σ=2). The outline of the CRF was defined as the contour isoline at 80% of the maximum response using MATLAB function 'contour3'. Neurons with only 1 contour region at the threshold were selected.

Data acquisition and spike sorting

Raw spike-band data were sampled and recorded at 30kHz. They were then median-subtracted and high-pass filtered at 300 Hz during the pre-processing stage. Spike sorting was carried out with Kilosort 3 (Pachitariu et al., 2024) to find spike times and assign each spike to different templates (neurons). Default parameters in Kilosort 3 were used for spike sorting, specifically, Ops.th = [9,9]; Ops.lam = 20; Ops.AUCsplit = 0.8; Ops.ThPre = 8; Ops.sig = 20; Ops.nblocks = 5; Ops.spkTh = −6. The raw sorted data were then manually curated in Phy (*https://github.com/cortex-lab/phy*) to remove templates with very few spikes or with atypical waveforms and to perform minimal templates merging and splitting. Double-counted spikes from the algorithm fitting the residuals to a new template were identified using established criteria (Siegle et al., 2021), by

counting spikes from two templates separated by less than 50μm (~5 channels) and with spike activity occurring within 5 samples (0.167ms). Double-counted spikes from the template smaller in amplitude were removed from further analysis. Visual responsiveness of each unit was assessed under CRF, nCRF, or RF mapping stimulation. For each type of stimulation, a paired-sample t test was performed to determine whether the mean spike counts after each stimulus presentation exceeded the preceding blank period at a significance level of 0.01. Only neurons showing significant visual responsiveness were included for further analysis.

Layer Assignment

The laminar locations of our recorded neurons were estimated based on a combination of functional analysis and histology results (Zhu et al., 2024; Carr et al., 2025). For each recording, we first performed the current source density (CSD) analysis on the stimulus-triggered average of local field potentials (LFP). LFP were low-pass filtered at 200 Hz and recorded at 2500 Hz. LFP signals recorded from every 4 nearby channels were averaged and realigned to the onset of visual stimulus. CSD was estimated as the second-order derivatives of signals along the probe axis using the common five-point formula (Nicholson and Freeman, 1975). The result was then smoothed across space (σ = 120 μm) to reduce the artifacts caused by varied electrode impedance. We located the lower boundary of the major sink (the reversal point of sink and source) as the border between layer 4C and layer 5/6. We also considered anatomical data in order to localize recorded neurons within gray matter, allowing for minor adjustments (±1 group channel) in layer boundary placement. Subsequent layer boundaries were determined by offsetting the cortical thickness derived from histological slices (Supplementary Fig S1).

Single neuron properties during CRF stimulation

To assess the orientation tuning for each neuron, the spike rates during 0.1 to 1s after each stimulus onset were calculated and averaged for each orientation condition (N= 18). The orientation tuning responses were first smoothed with a Hanning window (half-width at half-height of 20°), and then fitted with a von Mises function (Swindale, 1998)

$$y = a_0 + a_1 * e^{a_2*(\cos(2*x-2*a_3)-1)}$$

The location of the peak of the fitted curve was determined as the preferred orientation. Only neurons well fit by the function (R^2>0.7) were included for determining pairwise differences in preferences for all combinations in each recording session.

Modulation index for border ownership

As in previous studies (Zhou et al., 2000), we calculated a B_{own} modulation index to quantify the selectivity of each neuron for B_{own}. The B_{own} modulation index is defined as

$$B_{own}\ index = \frac{0.5 * (R_{LC1} + R_{LC2})_{Side1} - 0.5 * (R_{LC1} + R_{LC2})_{Side2}}{R_{max}}$$

Here, $R_{LC,\ Side}$ represents the average spike rate from 0.05 to 0.5 s after stimulus onset for one of four basic conditions, which are derived from the combination of two different *Local Contrast* conditions (LC1 and LC2) and two *Side* conditions (Side 1 and Side 2). Baseline activity was not subtracted. Since the border within the CRF can vary in 45° steps from 0° to 180°, we only selected the optimal orientation for each recording population to calculate the B_{own} index. R_{max} was defined as the maximum response for each neuron across the four basic conditions and four orientations. We used R_{max} instead of summing responses across the four basic conditions to account for the slight variations in orientation preferences among neurons within each recording session. The statistical significance of B_{own} was evaluated using a two-factor ANOVA (MATLAB function 'anovan') on the average spike rates for each condition. The two factors were object *Side* (with two levels: Side 1 and Side 2) and *Local Contrast* (with two levels: LC 1 and LC2), including

their interactions. A significance level of 0.05 was used. Neurons were considered to exhibit significant B_{own} modulation if they showed a significant main effect for the object *Side* factor. Whether they were invariant to local contrast was determined by the main effect of the *Local Contrast* factor.

Cross-correlograms (CCGs)

To measure correlated firing, we computed the cross-correlations between spike trains of all pairs of simultaneously recorded neurons. For each recording session, we calculated cross-correlograms (CCGs) from pairwise combinations of neuronal spike trains during either CRF (Gabor gratings) or nCRF (border ownership) stimulation conditions, respectively. We only included neuronal pairs with geometric mean firing rates more than 0.5 spikes/sec for further analysis. For both conditions, we focused on the spiking activity within the 0.25 −1s window during each stimulus presentation, to mitigate the influence of the transient visual response after stimulus onset. The CCG function for a given pair of neurons was defined as follows:

$$CCG(\tau)_{j-k} = \frac{\frac{1}{M}\sum_{i=1}^{M}\sum_{t=1}^{N-\tau} x_j^i(t) \times x_k^i(t+\tau)}{\theta(\tau)\sqrt{\lambda_j \lambda_k}}$$

where *j* denotes the first/reference neuron and *k* denotes the second/target neuron in the CCG function. τ is the time lag between the two spike trains x_j^i and x_k^i from neuron *j* and *k*, during trial *i*. The value of $x_j^i(t)$ and $x_k^i(t)$ is 1 if there is a spike at time bin *t* and is zero otherwise. *M* is the total number of trials; *N* is the number of time bins within a trial. $\theta(\tau) = N - |\tau|$, is a triangular function that corrects for the degree of overlap in the two spike trains at each time lag. λ_9 and λ: are the mean firing rates of neuron *j* and *k* computed over the same bins used to compute the CCG at each time lag. The normalization by the geometric mean of spike rates is commonly used by previous studies to account for the influence of firing rates on the CCG peaks (Bair et al., 2001; Kohn and Smith, 2005).

To correct for correlations due to stimulus-locking or slow fluctuations in the population responses (e.g., gamma-band activity), we computed a jitter-corrected CCG by subtracting a jittered CCG from the original CCG:

$$CCG_{corrected} = CCG_{original} - CCG_{jittered}$$

The jittered CCG ($CCG_{jittered}$) reflects the expected value of CCG computed from all possible jitters of each spike train within a given jitter window (Harrison and Geman, 2009; Smith and Kohn, 2008). The jittered spike train preserves both the PSTH of the original spike train across trials and the spike counts in the jitter window within each trial. As a result, jitter correction removes the correlation between PSTHs (stimulus-locking) and correlation on timescales longer than the jitter window (slow population correlations). Here, a 25-ms jitter window was chosen based on previous studies (Jia et al., 2013; Siegle et al., 2021). Jitter-corrected CCG ($CCG_{corrected}$) was then smoothed with a 5ms kernel [0.05, 0.25, 0.4, 0.25, 0.05] (Kohn and Smith, 2005; Smith and Kohn, 2008) before further analysis.

We classified a CCG as significant if the peak of the jitter-corrected CCG occurred within 10 ms of zero and exceeded 7 standard deviations (SD) above the mean of the noise distribution, similar to previous studies (Siegle et al., 2021). The noise distribution for a CCG was defined as the flanks of the jitter-corrected CCG ($\{CCG(\tau) | 100 \geq |\tau| \geq 50\ ms\}$). All analyses presented in the main text involve only significant, jitter-corrected CCGs. In the supplementary material, we also applied a more stringent criterion, requiring that significant CCG peaks exceed 10 SD above the noise, and a less stringent criterion that includes both significant and non-significant CCGs. These ensure that our results are robust across the choices of threshold (**Supplementary Figure S2**). To assess the directionality of functional interactions or signal flow between pairs of neurons, we focused on two metrics derived from the CCG functions. One is the peak lag (PL), which describes the time lag

of peak correlation between the spike trains of neuron *k* (target) relative to neuron *j* (reference). PL is positive if the reference neuron *j* leads target neuron *k* in spike timing, negative if *j* lags *k*, and zero if j and k fire synchronously. The second metric we used to assess the signal flow is CCG asymmetry, computed by subtracting the sum of CCG values during the [-13, 0] ms time window from the sum of CCG values during the [0, 13] ms. Similar to PL, a positive CCG asymmetry indicates that reference neuron *j* leads *k*, while a negative asymmetry indicates that *j* lags *k*. The 13ms window was chosen as half of the 25ms jitter window, consistent with previous studies (Jia et al., 2022). Compared to peak lag, CCG asymmetry additionally captures the strength of the functional interactions between pairs of neurons and is less dependent on the exact shape of the CCG peak, which is often more complex in corticocortical functional interactions (Alonso and Martinez, 1998).

Relationship between B_{own} modulation and interlaminar signal flow

To determine whether the magnitude of border ownership or local contrast modulation is predicted by interlaminar signal flow during nCRF stimulation, we first performed linear regression (MATLAB, 'fitlm', ordinary least squares) and then built generalized linear models (GLMs) using predictors including CCG asymmetry, interlaminar combinations, and recording sessions. We focused on the four key interlaminar combinations (4C-2/3, 4A/B-2/3, 4C-5/6, 4A/B-5/6), where the latter laminar compartments receive feedback/horizontal inputs (FH_i). Only neuronal pairs with significant CCGs were included as individual samples in the GLM. The resulting GLM equations were:

$$B_{own}(pair) \sim 1 + asymmetry + \ laminar\ combination + pen$$

$$LC(pair) \sim 1 + asymmetry + \ laminar\ combination + pen$$

B_{own} (pair) and LC (pair) were calculated as the geometric mean of the B_{own} and LC indices for the constituent neurons in each pair. Specifically, $B_{own}(pair) = \sqrt{abs(B_{own}(j)) * abs(B_{own}(k))}$, where abs($B_{own}(j)$) and abs($B_{own}(k)$) represent the absolute B_{own} modulation indices for constituent neurons *j* and *k*. A similar calculation was performed for LC (pair). CCG asymmetries were calculated from the nCRF stimulation condition where neurons in the input layers were selected as reference neurons and the ones in FH_i compartments were target neurons in the CCG. Additional predictors, including interlaminar combinations and recording sessions, were included in the models to incorporate variations when pooling the dataset.

Statistical tests

B_{own} for each neuron was assessed with ANOVA. The proportion of B_{own} neurons within different layers was assessed using chi-squared test of homogeneity. The sign of populational border ownership preferences from individual recording session was tested with sign test. The sign of populational CCG peak lag for a given laminar compartment combination was assessed with sign test. The comparisons of peak lag and CCG asymmetry between CRF and nCRF stimulation condition for each laminar compartment combination were evaluated using Wilcoxon rank-sum tests. The dependence between CCG asymmetry and B_{own} for pair of neurons was assessed using linear regression and GLM.

Supplementary figure legends and tables

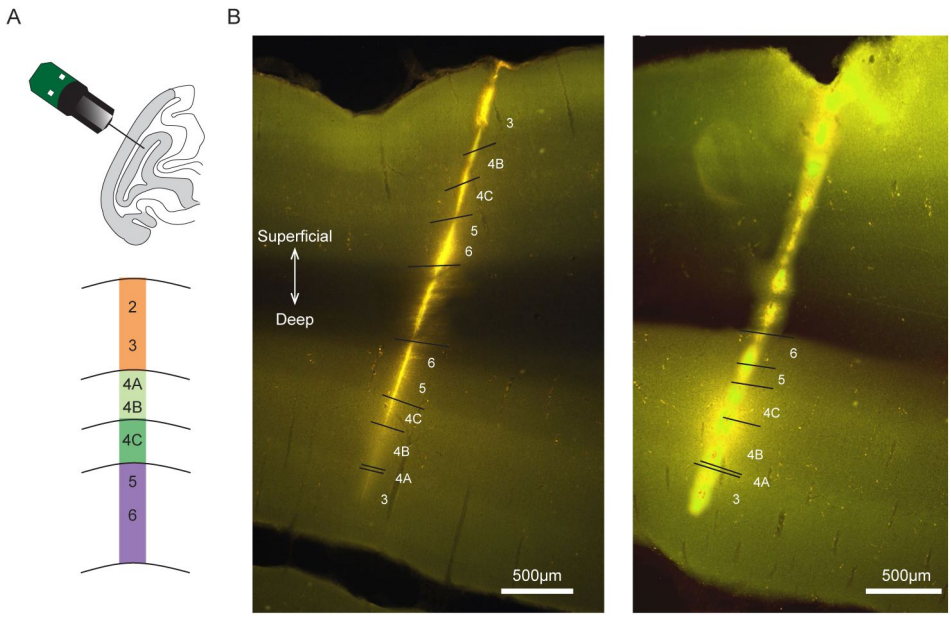

Supplementary Figure S1.

Histological data for Neuropixels recordings in macaque V1

(A) Neuropixels probe (384 channels/3.84mm) penetrations made into the lateral surface or underlying calcarine sulcus of macaque V1. Bottom: Diagram of designated laminar compartments. (B) Histological reconstruction of probe tracks based on DiI derivative staining for two example recordings (*pen3-4*). Here, Neuropixels probes passed through the lateral surface and reached the calcarine sulcus of V1. Only neurons in the calcarine V1 from these two recordings were tested and included in the analysis. Designated boundaries are shown. Scale bar, 500 μm.

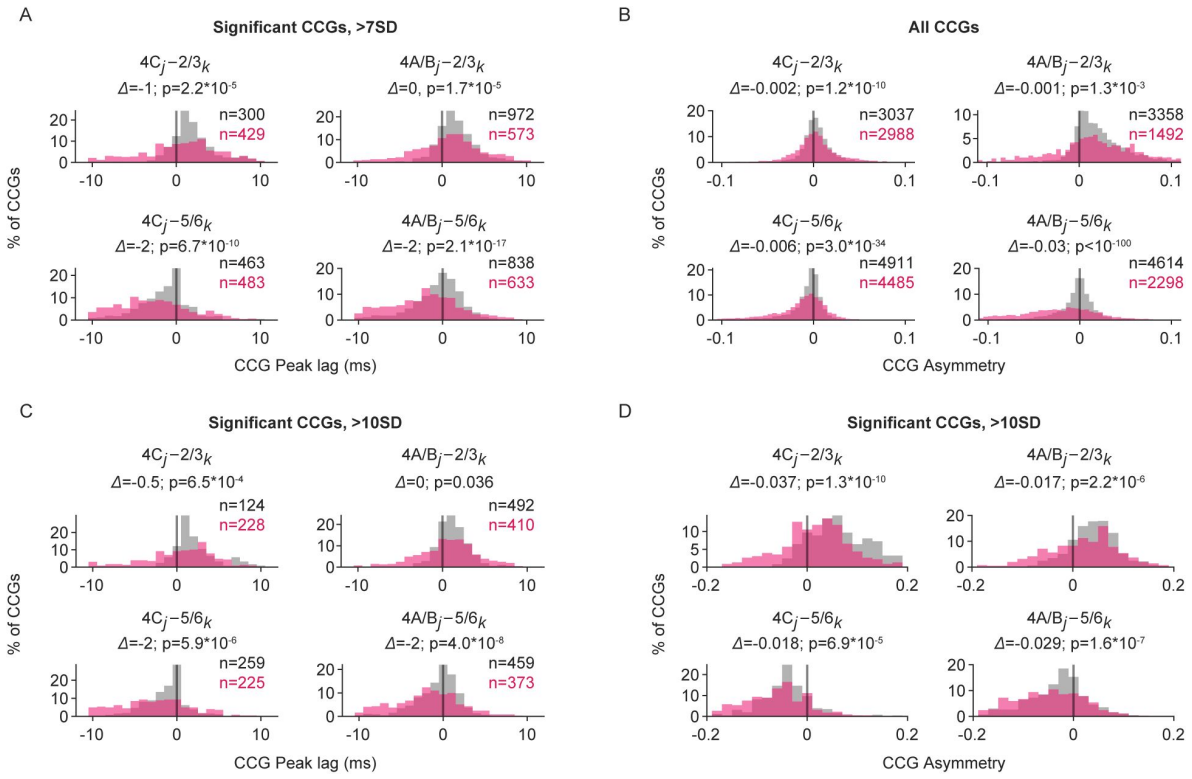

Supplementary Figure S2.

Comparison of interlaminar cross-correlations during CRF and nCRF stimulation under different CCG criteria

(A) Histogram distributions of CCG peak lags for each of the four key interlaminar combinations in the combined dataset during CRF (gray) and nCRF (magenta) stimulation. The shift (β) in median CCG peak lags during nCRF stimulation relative to CRF stimulation is shown. Significant CCGs are defined as those with peaks exceeding 7 SD above the noise level (flank). (B) Similar to (A), but comparing CCG asymmetry across all CCGs, including both significant and non-significant ones. (C) Comparison of CCG peak lags using a stricter criterion, where significant CCGs are defined as those with peaks exceeding 10 SD above the noise level (flank). (D) Comparison of CCG asymmetry using the stricter criterion of 10 SD.

Table S1.

Number of neurons selective to B_{own} (LC) across recordings

Layer	Total	p_{Side} <0.05		p_{Side} ≥0.05		Layer	Total	p_{Side} <0.05		p_{Side} ≥0.05	
		p_{LC} ≥0.05	p_{LC} <0.05	p_{LC} <0.05	p_{LC} ≥0.05			p_{LC} ≥0.05	p_{LC} <0.05	p_{LC} <0.05	p_{LC} ≥0.05
	pen1						***pen2***				
2/3	29	6	5	6	12	2/3	55	1	14	18	22
4A/B	19	0	5	8	6	4A/B	34	0	7	10	17
4C	38	3	7	16	12	4C	54	4	15	22	13
5/6	40	2	7	18	13	5/6	27	5	2	4	16
	pen3						***pen4***				
2/3	15	1	1	4	9	2/3	0	0	0	0	0
4A/B	27	0	4	9	14	4A/B	34	3	0	2	29
4C	60	1	12	24	23	4C	60	2	4	5	49
5/6	40	2	7	2	29	5/6	37	3	0	2	32
	pen all										
2/3	99	8	20	28	43						
4A/B	114	3	16	29	66						
4C	212	10	38	67	97						
5/6	144	12	16	26	90						

Table S2.

Comparison of CCG asymmetries during CRF and nCRF for each recording

4C-2/3	*CRF*	*nCRF*	**Δ**	***p***	**4A/B-2/3**	*CRF*	*nCRF*	**Δ**	***p***
*pen*1	0.036	-0.004	-0.040	$2.8*10^{-7}$	*pen*1	0.046	-0.005	-0.050	$7.5*10^{-12}$
pen2	0.037	0.013	-0.024	$3.7*10^{-9}$	*pen2*	0.030	0.022	-0.008	0.066
pen3	0.017	0.033	0.016	0.29	*pen3*	0.049	0.052	0.003	0.99
4C-5/6	*CRF*	*nCRF*	**Δ**	***p***	**4A/B-5/6**	*CRF*	*nCRF*	**Δ**	***p***
*pen*1	-0.010	-0.044	-0.033	0.0015	*pen*1	0.012	-0.028	-0.040	$2.1*10^{-6}$
pen2	-0.009	-0.027	-0.018	$1.5*10^{-5}$	*pen2*	-0.011	-0.018	-0.007	0.059
pen3	-0.036	-0.062	-0.026	$5.8*10^{-7}$	*pen3*	-0.025	-0.087	-0.063	$9.1*10^{-15}$
pen4	-0.041	-0.093	-0.051	$3.1*10^{-8}$	*pen4*	-0.030	-0.089	-0.060	$9.1*10^{-12}$

Table S3.

GLMs for dependence of border ownership and local contrast on CCG asymmetry

$$B_{own}(pair) \sim 1 + CCG\ asymmetry + \ laminar\ combination + pen$$

$$LC(pair) \sim 1 + CCG\ asymmetry + \ laminar\ combination + pen$$

GLM	Border ownership (B_{own})				Local contrast (LC)			
	Estimate	SE	tStat	p	Estimate	SE	tStat	p
Intercept	0.166	0.008	21.379	0	0.362	0.010	35.352	0
CCG asymmetry	**-0.158**	0.032	-4.880	**$1.1*10^{-6}$**	**-0.044**	0.043	-1.037	**0.300**
4C-5/6 *rel.4C-2/3*	0.014	0.007	1.948	0.05	-0.117	0.009	-12.606	$3.5*10^{-35}$
4A/B-2/3 *rel.4C-2/3*	$2.5*10^{-5}$	0.006	0.004	0.99	-0.016	0.008	-1.877	0.061
4A/B-5/6 *rel.4C-2/3*	0.009	0.007	1.351	0.18	-0.136	0.009	-15.093	0
$pen2_{rel.pen1}$	-0.009	0.007	-1.219	0.22	0.010	0.010	0.980	0.327
$pen3_{rel.pen1}$	0.038	0.009	4.435	$9.7*10^{-6}$	0.035	0.011	3.082	0.002
$pen4_{rel.pen1}$	0.049	0.010	5.147	$2.9*10^{-7}$	-0.088	0.013	-6.910	$6.4*10^{-12}$

Number of observations: 2118; Error degrees of freedom: 2110

GLM(B_{own}): R^2=0.11; F-statistic vs. constant model: 37.2, p-value=0.

GLM(LC): R^2=0.27; F-statistic vs. constant model: 109, p-value=0.

Acknowledgements

We thank Jonathan C. Horton for extensive help with the recordings and histology, Danielle A. Lopes, Stephen Cital, Shellie Hyde and Sam Baker for technical assistance, Tim Harris and Karel Svoboda for providing the Neuropixels probes. This work was supported by NIH Grant EY029759, Brain and Behavior Research Foundation Grant to X.M.; NIH Grants EY014924, NS116623, and a Ben Barres Professorship to T.M.

Additional information

Data and Code Availability

All raw data generated in this study will be deposited in a public repository upon acceptance and made publicly available prior to publication.

The code developed for data analysis has been deposited to GitHub (*https://github.com/szhu-007/Zhu_V1_interlaminar-signal-flow*) and is freely available for access.

Author Contributions

Conceptualization, S.Z., X.C. and T.M.; Investigation, S.Z., X.C. and T.M.; Software, S.Z. and E.T.; Formal Analysis, S.Z. and Y.J.O.; Visualization, S.Z., Y.J.O.; Writing – Original Draft, S.Z. and T.M.; Writing – Review and Editing, S.Z., Y.J.O., E.T., X.C., T.M.; Funding Acquisition, X.C. and T.M.

Funding

National Institutes of Health (EY029759)

National Institutes of Health (EY014924)

National Institutes of Health (NS116623)

Brain & Behavior Research Foundation

Ben Barres Professorship

References

Adesnik H., Bruns W., Taniguchi H., Huang Z. J., Scanziani M (2012) **A neural circuit for spatial summation in visual cortex** *Nature* **490**:226–31 Google Scholar

Aertsen A. M., Gerstein G. L (1985) **Evaluation of neuronal connectivity: sensitivity of cross-correlation** *Brain Res* **340**:341–54 Google Scholar

Albright T. D., Stoner G. R (2002) **Contextual influences on visual processing** *Annu Rev Neurosci* **25**:339–79 Google Scholar

Allman J., Miezin F., Mcguinness E (1985) **Stimulus specific responses from beyond the classical receptive field: neurophysiological mechanisms for local-global comparisons in visual neurons** *Annu Rev Neurosci* **8**:407–30 Google Scholar

Alonso J., Chen Y (2009) **Receptive field** *Scholarpedia* **4**:5393 Google Scholar

Alonso J. M., Martinez L. M (1998) **Functional connectivity between simple cells and complex cells in cat striate cortex** *Nature Neuroscience* **1**:395–403 Google Scholar

Alonso J. M., Usrey W. M., Reid R. C (1996) **Precisely correlated firing in cells of the lateral geniculate nucleus** *Nature* **383**:815–9 Google Scholar

Anderson J. C., Martin K. A (2009) **The synaptic connections between cortical areas V1 and V2 in macaque monkey** *J Neurosci* **29**:11283–93 Google Scholar

Andrews T. J., Schluppeck D., Homfray D., Matthews P., Blakemore C (2002) **Activity in the fusiform gyrus predicts conscious perception of Rubin's vase-face illusion** *Neuroimage* **17**:890–901 Google Scholar

Angelucci A., Bijanzadeh M., Nurminen L., Federer F., Merlin S., Bressloff P. C (2017) **Circuits and Mechanisms for Surround Modulation in Visual Cortex** *Annu Rev Neurosci* **40**:425–451 Google Scholar

Angelucci A., Bressloff P. C (2006) **Contribution of feedforward, lateral and feedback connections to the classical receptive field center and extra-classical receptive field surround of primate V1 neurons** *Prog Brain Res* **154**:93–120 Google Scholar

Angelucci A., Levitt J. B., Walton E. J., Hupe J. M., Bullier J., Lund J. S (2002) **Circuits for local and global signal integration in primary visual cortex** *J Neurosci* **22**:8633–46 Google Scholar

Bair W., Cavanaugh J. R., Movshon J. A (2003) **Time course and time-distance relationships for surround suppression in macaque V1 neurons** *J Neurosci* **23**:7690–701 Google Scholar

Bair W., Zohary E., Newsome W. T (2001) **Correlated firing in macaque visual area MT: time scales and relationship to behavior** *J Neurosci* **21**:1676–97 Google Scholar

Bijanzadeh M., Nurminen L., Merlin S., Clark A. M., Angelucci A (2018) **Distinct Laminar Processing of Local and Global Context in Primate Primary Visual Cortex** *Neuron* **100**:259–274 Google Scholar

Blasdel G. G., Lund J. S (1983) **Termination of afferent axons in macaque striate cortex** *J Neurosci* **3**:1389–413 Google Scholar

Blasdel G. G., Lund J. S., Fitzpatrick D (1985) **Intrinsic connections of macaque striate cortex: axonal projections of cells outside lamina 4C** *J Neurosci* **5**:3350–69 Google Scholar

Briggs F., Mangun G. R., Usrey W. M (2013) **Attention enhances synaptic efficacy and the signal-to-noise ratio in neural circuits** *Nature* **499**:476–80 Google Scholar

Bringuier V., Chavane F., Glaeser L., Fregnac Y (1999) **Horizontal propagation of visual activity in the synaptic integration field of area 17 neurons** *Science* **283**:695–9 Google Scholar

Bullier J., Hupe J. M., James A. C., Girard P (2001) **The role of feedback connections in shaping the responses of visual cortical neurons** *Prog Brain Res* **134**:193–204 Google Scholar

Callaway E. M (1998) **Local circuits in primary visual cortex of the macaque monkey** *Annu Rev Neurosci* **21**:47–74 Google Scholar

Callaway E. M (2004) **Feedforward, feedback and inhibitory connections in primate visual cortex** *Neural Netw* **17**:625–32 Google Scholar

Callaway E. M., Wiser A. K (1996) **Contributions of individual layer 2-5 spiny neurons to local circuits in macaque primary visual cortex** *Vis Neurosci* **13**:907–22 Google Scholar

Carr N., Zhu S., Chen X., Lee K., Perliss A., Moore T., Chandrasekaran C (2025) **Neuropixels reveal structure-function relationships in monkey V1 in vivo** *bioRxiv* Google Scholar

Chen M., Yan Y., Gong X., Gilbert C. D., Liang H., Li W (2014) **Incremental integration of global contours through interplay between visual cortical areas** *Neuron* **82**:682–94 Google Scholar

Chen R., Wang F., Liang H., Li W (2017) **Synergistic Processing of Visual Contours across Cortical Layers in V1 and V2** *Neuron* **96**:1388–1402 Google Scholar

Chisum H. J., Mooser F., Fitzpatrick D (2003) **Emergent properties of layer 2/3 neurons reflect the collinear arrangement of horizontal connections in tree shrew visual cortex** *J Neurosci* **23**:2947–60 Google Scholar

Chu C. C., Chien P. F., Hung C. P (2014) **Tuning dissimilarity explains short distance decline of spontaneous spike correlation in macaque V1** *Vision Res* **96**:113–32 Google Scholar

Craft E., Schütze H., Niebur E., Von Der Heydt R. (2007) **A neural model of figure-ground organization** *J. Neurophysiol* **97**:4310–4326 Google Scholar

Denman D. J., Contreras D (2014) **The structure of pairwise correlation in mouse primary visual cortex reveals functional organization in the absence of an orientation map** *Cereb Cortex* **24**:2707–20 Google Scholar

Eguchi A., Stringer S. M (2016) **Neural network model develops border ownership representation through visually guided learning** *Neurobiol Learn Mem* **136**:147–165 Google Scholar

Fang F., Boyaci H., Kersten D (2009) **Border ownership selectivity in human early visual cortex and its modulation by attention** *J Neurosci* **29**:460–5 Google Scholar

Federer F., TA'afua S., Merlin S., Hassanpour M. S., Angelucci A. (2021) **Stream-specific feedback inputs to the primate primary visual cortex** *Nat Commun* **12**:228 Google Scholar

Fitzpatrick D (2000) **Seeing beyond the receptive field in primary visual cortex** *Curr Opin Neurobiol* **10**:438–43 Google Scholar

Fitzpatrick D., Lund J. S., Blasdel G. G (1985) **Intrinsic connections of macaque striate cortex: afferent and efferent connections of lamina 4C** *J Neurosci* **5**:3329–49 Google Scholar

Franken T. P., Reynolds J. H (2021) **Columnar processing of border ownership in primate visual cortex** *eLife* **10** Google Scholar

Gieselmann M. A., Thiele A (2022) **Stimulus dependence of directed information exchange between cortical layers in macaque V1** *eLife* **11** Google Scholar

Gilbert C. D., Wiesel T. N (1983) **Clustered intrinsic connections in cat visual cortex** *J Neurosci* **3**:1116–33 Google Scholar

Gilbert C. D., Wiesel T. N (1990) **The influence of contextual stimuli on the orientation selectivity of cells in primary visual cortex of the cat** *Vision Res* **30**:1689–701 Google Scholar

Girard P., Hupe J. M., Bullier J (2001) **Feedforward and feedback connections between areas V1 and V2 of the monkey have similar rapid conduction velocities** *J Neurophysiol* **85**:1328–31 Google Scholar

Grinvald A., Lieke E. E., Frostig R. D., Hildesheim R (1994) **Cortical point-spread function and long-range lateral interactions revealed by real-time optical imaging of macaque monkey primary visual cortex** *J Neurosci* **14**:2545–68 Google Scholar

Gur M., Kagan I., Snodderly D. M (2005) **Orientation and direction selectivity of neurons in V1 of alert monkeys: functional relationships and laminar distributions** *Cereb Cortex* **15**:1207–21 Google Scholar

Hansen B. J., Chelaru M. I., Dragoi V (2012) **Correlated variability in laminar cortical circuits** *Neuron* **76**:590–602 Google Scholar

Harrison M. T., Geman S (2009) **A rate and history-preserving resampling algorithm for neural spike trains** *Neural Comput* **21**:1244–58 Google Scholar

Hartline H. K (1938) **The response of single optic nerve fibers of the vertebrate eye to illumination of the retina** *American Journal of Physiology-Legacy Content* **121**:400–415 Google Scholar

Hembrook-Short J. R., Mock V. L., Usrey W. M., Briggs F (2019) **Attention Enhances the Efficacy of Communication in V1 Local Circuits** *J Neurosci* **39**:1066–1076 Google Scholar

Hendrickson A. E., Wilson J. R., Ogren M. P (1978) **The neuroanatomical organization of pathways between the dorsal lateral geniculate nucleus and visual cortex in Old World and New World primates** *J Comp Neurol* **182**:123–36 Google Scholar

Henry C. A., Joshi S., Xing D., Shapley R. M., Hawken M. J (2013) **Functional characterization of the extraclassical receptive field in macaque V1: contrast, orientation, and temporal dynamics** *J Neurosci* **33**:6230–42 Google Scholar

Hesse J. K., Tsao D. Y (2016) **Consistency of Border-Ownership Cells across Artificial Stimuli, Natural Stimuli, and Stimuli with Ambiguous Contours** *J Neurosci* **36**:11338–11349 Google Scholar

Hesse J. K., Tsao D. Y (2023) **Functional modules for visual scene segmentation in macaque visual cortex** *Proc Natl Acad Sci U S A* **120**:e2221122120 Google Scholar

Hirabayashi T., Miyashita Y (2005) **Dynamically modulated spike correlation in monkey inferior temporal cortex depending on the feature configuration within a whole object** *J Neurosci* **25**:10299–307 Google Scholar

Hirabayashi T., Takeuchi D., Tamura K., Miyashita Y. (2010) **Triphasic dynamics of stimulus-dependent information flow between single neurons in macaque inferior temporal cortex** *J Neurosci* **30**:10407–21 Google Scholar

Huang L., Wang L., Shen W., Li M., Wang S., Wang X., Ungerleider L. G., Zhang X (2020) **A source for awareness-dependent figure-ground segregation in human prefrontal cortex** *Proc Natl Acad Sci U S A* **117**:30836–30847 Google Scholar

Hubel D. H., Wiesel T. N (1972) **Laminar and columnar distribution of geniculo-cortical fibers in the macaque monkey** *J Comp Neurol* **146**:421–50 Google Scholar

Hung C. P., Ramsden B. M., Roe A. W (2007) **A functional circuitry for edge-induced brightness perception** *Nat Neurosci* **10**:1185–90 Google Scholar

Hupe J. M., James A. C., Girard P., Lomber S. G., Payne B. R., Bullier J (2001) **Feedback connections act on the early part of the responses in monkey visual cortex** *J Neurophysiol* **85**:134–45 Google Scholar

Hupe J. M., James A. C., Payne B. R., Lomber S. G., Girard P., Bullier J (1998) **Cortical feedback improves discrimination between figure and background by V1, V2 and V3 neurons** *Nature* **394**:784–7 Google Scholar

Ichida J. M., Schwabe L., Bressloff P. C., Angelucci A (2007) **Response facilitation from the "suppressive" receptive field surround of macaque V1 neurons** *J Neurophysiol* **98**:2168–81 Google Scholar

Jehee J. F., Lamme V. A., Roelfsema P. R (2007) **Boundary assignment in a recurrent network architecture** *Vision Res* **47**:1153–65 Google Scholar

Jeurissen D., Self M. W., Roelfsema P. R (2016) **Serial grouping of 2d-image regions with object-based attention in humans** *eLife* **5** Google Scholar

Jia X., Tanabe S., Kohn A (2013) **. gamma and the coordination of spiking activity in early visual cortex** *Neuron* **77**:762–74 Google Scholar

Jia X. X., Siegle J. H., Durand S., Heller G., Ramirez T. K., Koch C., Olsen S. R (2022) **Multi-regional module-based signal transmission in mouse visual cortex** *Neuron* **110**:1585 Google Scholar

Jones H. E., Andolina I. M., Shipp S. D., Adams D. L., Cudeiro J., Salt T. E., Sillito A. M (2015) **Figure-ground modulation in awake primate thalamus** *Proc Natl Acad Sci U S A* **112**:7085–90 Google Scholar

Jun J. J., Steinmetz N. A., Siegle J. H., Denman D. J., Bauza M., Barbarits B., Lee A. K., Anastassiou C. A., Andrei A., Aydin C., Barbic M., Blanche T. J., Bonin V., Couto J., Dutta B., Gratiy S. L., Gutnisky D. A., Hausser M., Karsh B., Ledochowitsch P., Lopez C. M., Mitelut C., Musa S., Okun M., Pachitariu M., Putzeys J., Rich P. D., Rossant C., Sun W. L., Svoboda K., Carandini M., Harris K. D., Koch C., O'keefe J., Harris T. D (2017) **Fully integrated silicon probes for high-density recording of neural activity** *Nature* **551**:232–236 Google Scholar

Kapadia M. K., Ito M., Gilbert C. D., Westheimer G (1995) **Improvement in visual sensitivity by changes in local context: parallel studies in human observers and in V1 of alert monkeys** *Neuron* **15**:843–56 Google Scholar

Keller A. J., Roth M. M., Scanziani M (2020) **Feedback generates a second receptive field in neurons of the visual cortex** *Nature* **582**:545–549 Google Scholar

Kleiner M., Brainard D., Pelli D (2007) **What's new in Psychtoolbox-3?** *Perception* **36**:14–14 Google Scholar

Klink P. C., Dagnino B., Gariel-Mathis M. A., Roelfsema P. R (2017) **Distinct Feedforward and Feedback Effects of Microstimulation in Visual Cortex Reveal Neural Mechanisms of Texture Segregation** *Neuron* **95**:209–220 Google Scholar

Knierim J. J., Van Essen D. C. (1992) **Neuronal responses to static texture patterns in area V1 of the alert macaque monkey** *J Neurophysiol* **67**:961–80 Google Scholar

Ko H. K., Von Der Heydt R. (2018) **Figure-ground organization in the visual cortex: does meaning matter?** *J Neurophysiol* **119**:160–176 Google Scholar

Kogo N., Strecha C., Van Gool L., & Wagemans J. (2010) **Surface construction by a 2-D differentiation-integration process: a neurocomputational model for perceived border ownership, depth, and lightness in Kanizsa figures** *Psychol Rev* **117**:406–39 Google Scholar

Kohn A., Smith M. A (2005) **Stimulus dependence of neuronal correlation in primary visual cortex of the macaque** *J Neurosci* **25**:3661–73 Google Scholar

Kourtzi Z., Kanwisher N (2001) **Representation of perceived object shape by the human lateral occipital complex** *Science* **293**:1506–9 Google Scholar

Lamme V. A (1995) **The neurophysiology of figure-ground segregation in primary visual cortex** *J Neurosci* **15**:1605–15 Google Scholar

Lamme V. A., Zipser K., Spekreijse H (1998) **Figure-ground activity in primary visual cortex is suppressed by anesthesia** *Proc Natl Acad Sci U S A* **95**:3263–8 Google Scholar

Layton O. W., Mingolla E., Yazdanbakhsh A (2012) **Dynamic coding of border-ownership in visual cortex** *J Vis* **12**:8 Google Scholar

Lee T. S., Yang C. F., Romero R. D., Mumford D (2002) **Neural activity in early visual cortex reflects behavioral experience and higher-order perceptual saliency** *Nat Neurosci* **5**:589–97 Google Scholar

Li W., Piech V., Gilbert C. D (2006) **Contour saliency in primary visual cortex** *Neuron* **50**:951–62 Google Scholar

Li Y., Wang T., Yang Y., Dai W., Wu Y., Li L., Han C., Zhong L., Li L., Wang G., Dou F., Xing D (2022) **Cascaded normalizations for spatial integration in the primary visual cortex of primates** *Cell Rep* **40**:111221 Google Scholar

Liang H., Gong X., Chen M., Yan Y., Li W., Gilbert C. D (2017) **Interactions between feedback and lateral connections in the primary visual cortex** *Proc Natl Acad Sci U S A* **114**:8637–8642 Google Scholar

Lund J. S (1973) **Organization of neurons in the visual cortex, area 17, of the monkey (Macaca mulatta)** *J Comp Neurol* **147**:455–96 Google Scholar

Lund J. S (1988) **Anatomical organization of macaque monkey striate visual cortex** *Annu Rev Neurosci* **11**:253–88 Google Scholar

Lund J. S., Yoshioka T (1991) **Local circuit neurons of macaque monkey striate cortex: III. Neurons of laminae 4b, 4a, and 3B** *J Comp Neurol* **311**:234–58 Google Scholar

Marcus D. S., Van Essen D. C. (2002) **Scene segmentation and attention in primate cortical areas V1 and V2** *J Neurophysiol* **88**:2648–58 Google Scholar

Markov N. T., Vezoli J., Chameau P., Falchier A., Quilodran R., Huissoud C., Lamy C., Misery P., Giroud P., Ullman S., Barone P., Dehay C., Knoblauch K., Kennedy H (2014) **Anatomy of hierarchy: feedforward and feedback pathways in macaque visual cortex** *J Comp Neurol* **522**:225–59 Google Scholar

Martin A. B., Von Der Heydt R. (2015) **Spike synchrony reveals emergence of proto-objects in visual cortex** *Journal of Neuroscience* **35**:6860–6870 Google Scholar

Mates S. L., Lund J. S (1983) **Neuronal composition and development in lamina 4C of monkey striate cortex** *J Comp Neurol* **221**:60–90 Google Scholar

Mehrani P., Tsotsos J. K (2021) **Early recurrence enables figure border ownership** *Vision Res* **186**:23–33 Google Scholar

Melssen W. J., Epping W. J (1987) **Detection and estimation of neural connectivity based on crosscorrelation analysis** *Biol Cybern* **57**:403–14 Google Scholar

Moore G. P., Segundo J. P., Perkel D. H., Levitan H (1970) **Statistical signs of synaptic interaction in neurons** *Biophys J* **10**:876–900 Google Scholar

Muller J. R., Metha A. B., Krauskopf J., Lennie P (2003) **Local signals from beyond the receptive fields of striate cortical neurons** *J Neurophysiol* **90**:822–31 Google Scholar

Nakayama K., He Z. J., Shimojo S (1995) **Visual Surface Representation: A Critical Link between Lower-Level and Higher-Level Vision** In: Kosslyn S. M., Osherson D. N., editors. *An Invitation to Cognitive Science, Volume 2: Visual Cognition* The MIT Press Google Scholar

Nandy A. S., Nassi J. J., Reynolds J. H (2017) **Laminar Organization of Attentional Modulation in Macaque Visual Area V4** *Neuron* **93**:235–246 Google Scholar

Nassi J. J., Lomber S. G., Born R. T (2013) **Corticocortical feedback contributes to surround suppression in V1 of the alert primate** *J Neurosci* **33**:8504–17 Google Scholar

Nelson J. I., Frost B. J (1985) **Intracortical facilitation among co-oriented, co-axially aligned simple cells in cat striate cortex** *Exp Brain Res* **61**:54–61 Google Scholar

Nelson J. I., Salin P. A., Munk M. H., Arzi M., Bullier J (1992) **Spatial and temporal coherence in cortico-cortical connections: a cross-correlation study in areas 17 and 18 in the cat** *Vis Neurosci* **9**:21–37 Google Scholar

Nicholson C., Freeman J. A (1975) **Theory of current source-density analysis and determination of conductivity tensor for anuran cerebellum** *J Neurophysiol* **38**:356–68 Google Scholar

Nothdurft H. C., Gallant J. L., Van Essen D. C. (1999) **Response modulation by texture surround in primate area V1: correlates of "popout" under anesthesia** *Vis Neurosci* **16**:15–34 Google Scholar

Nurminen L., Merlin S., Bijanzadeh M., Federer F., Angelucci A (2018) **Top-down feedback controls spatial summation and response amplitude in primate visual cortex** *Nat Commun* **9**:2281 Google Scholar

O'herron P. J., Von Der Heydt R. (2009) **Short-term memory for figure-ground organization in the visual cortex** *Neuron* **61**:801–809 Google Scholar

O'kusky J., Colonnier M (1982) **A laminar analysis of the number of neurons, glia, and synapses in the adult cortex (area 17) of adult macaque monkeys** *J Comp Neurol* **210**:278–90 Google Scholar

Ostojic S., Brunel N., Hakim V (2009) **How connectivity, background activity, and synaptic properties shape the cross-correlation between spike trains** *J Neurosci* **29**:10234–53 Google Scholar

Pachitariu M., Sridhar S., Pennington J., Stringer C (2024) **Spike sorting with Kilosort4** *Nat Methods* **21**:914–921 Google Scholar

Pak A., Ryu E., Li C., Chubykin A. A (2020) **Top-Down Feedback Controls the Cortical Representation of Illusory Contours in Mouse Primary Visual Cortex** *J Neurosci* **40**:648–660 Google Scholar

Perkel D. H., Gerstein G. L., Moore G. P (1967) **Neuronal spike trains and stochastic point processes. II. Simultaneous spike trains** *Biophys J* **7**:419–40 Google Scholar

Pettine W. W., Steinmetz N. A., Moore T (2019) **Laminar segregation of sensory coding and behavioral readout in macaque V4** *Proc Natl Acad Sci U S A* **116**:14749–14754 Google Scholar

Poltoratski S., Tong F (2020) **Resolving the Spatial Profile of Figure Enhancement in Human V1 through Population Receptive Field Modeling** *J Neurosci* **40**:3292–3303 Google Scholar

Poort J., Raudies F., Wannig A., Lamme V. A., Neumann H., Roelfsema P. R (2012) **The role of attention in figure-ground segregation in areas V1 and V4 of the visual cortex** *Neuron* **75**:143–56 Google Scholar

Qiu F. T., Sugihara T., Von Der Heydt R. (2007) **Figure-ground mechanisms provide structure for selective attention** *Nature Neuroscience* **10**:1492–1499 Google Scholar

Ramsden B. M., Hung C. P., Roe A. W (2001) **Real and illusory contour processing in area V1 of the primate: a cortical balancing act** *Cereb Cortex* **11**:648–65 Google Scholar

Reid R. C., Alonso J. M (1995) **Specificity of monosynaptic connections from thalamus to visual cortex** *Nature* **378**:281–4 Google Scholar

Rockland K. S., Lund J. S (1983) **Intrinsic laminar lattice connections in primate visual cortex** *J Comp Neurol* **216**:303–18 Google Scholar

Rockland K. S., Pandya D. N (1979) **Laminar origins and terminations of cortical connections of the occipital lobe in the rhesus monkey** *Brain Res* **179**:3–20 Google Scholar

Rockland K. S., Saleem K. S., Tanaka K (1994) **Divergent feedback connections from areas V4 and TEO in the macaque** *Vis Neurosci* **11**:579–600 Google Scholar

Rockland K. S., Virga A (1989) **Terminal arbors of individual "feedback" axons projecting from area V2 to V1 in the macaque monkey: a study using immunohistochemistry of anterogradely transported Phaseolus vulgaris-leucoagglutinin** *J Comp Neurol* **285**:54–72 Google Scholar

Roe A. W., TS'o D. Y. (1999) **Specificity of color connectivity between primate V1 and V2** *J Neurophysiol* **82**:2719–30 Google Scholar

Roelfsema P. R (2006) **Cortical algorithms for perceptual grouping** *Annu Rev Neurosci* **29**:203–27 Google Scholar

Sakai K., Nishimura H (2006) **Surrounding suppression and facilitation in the determination of border ownership** *J Cogn Neurosci* **18**:562–79 Google Scholar

Schwabe L., Obermayer K., Angelucci A., Bressloff P. C (2006) **The role of feedback in shaping the extra-classical receptive field of cortical neurons: a recurrent network model** *J Neurosci* **26**:9117–29 Google Scholar

Schwarz C., Bolz J (1991) **Functional specificity of a long-range horizontal connection in cat visual cortex: a cross-correlation study** *J Neurosci* **11**:2995–3007 Google Scholar

Self M. W., Jeurissen D., Van Ham A. F., Van Vugt B., Poort J., Roelfsema P. R. (2019) **The Segmentation of Proto-Objects in the Monkey Primary Visual Cortex** *Curr Biol* **29**:1019–1029 Google Scholar

Self M. W., Van Kerkoerle T., Super H., & Roelfsema P. R. (2013) **Distinct roles of the cortical layers of area V1 in figure-ground segregation** *Curr Biol* **23**:2121–9 Google Scholar

Senzai Y., Fernandez-Ruiz A., Buzsaki G (2019) **Layer-Specific Physiological Features and Interlaminar Interactions in the Primary Visual Cortex of the Mouse** *Neuron* **101**:500–513 Google Scholar

Shmuel A., Korman M., Sterkin A., Harel M., Ullman S., Malach R., Grinvald A (2005) **Retinotopic axis specificity and selective clustering of feedback projections from V2 to V1 in the owl monkey** *J Neurosci* **25**:2117–31 Google Scholar

Sibille J., Gehr C., Benichov J. I., Balasubramanian H., Teh K. L., Lupashina T., Vallentin D., Kremkow J (2022) **High-density electrode recordings reveal strong and specific connections between retinal ganglion cells and midbrain neurons** *Nature Communications* **13** Google Scholar

Siegle J. H., Jia X., Durand S., Gale S., Bennett C., Graddis N., Heller G., Ramirez T. K., Choi H., Luviano J. A., Groblewski P. A., Ahmed R., Arkhipov A., Bernard A., Billeh Y. N., Brown D., Buice M. A., Cain N., Caldejon S., Casal L., Cho A., Chvilicek M., Cox T. C., Dai K., Denman D. J., De Vries S. E. J., Dietzman R., Esposito L., Farrell C., Feng D., Galbraith J., Garrett M., Gelfand E. C., Hancock N., Harris J. A., Howard R., Hu B., Hytnen R., Iyer R., Jessett E., Johnson K., Kato I., Kiggins J., Lambert S., Lecoq J., Ledochowitsch P., Lee J. H., Leon A., Li Y., Liang E., Long F., Mace K., Melchior J., Millman D., Mollenkopf T., Nayan C., Ng L., Ngo K., Nguyen T., Nicovich P. R., North K., Ocker G. K., Ollerenshaw D., Oliver M., Pachitariu M., Perkins J., Reding M., Reid D., Robertson M., Ronellenfitch K., Seid S., Slaughterbeck C., Stoecklin M., Sullivan D., Sutton B., Swapp J., Thompson C., Turner K., Wakeman W., Whitesell J. D., Williams D., Williford A., Young R., Zeng H., Naylor S., Phillips J. W., Reid R. C., Mihalas S., Olsen S. R., Koch C. (2021) **Survey of spiking in the mouse visual system reveals functional hierarchy** *Nature* **592**:86–92 Google Scholar

Sillito A. M., Grieve K. L., Jones H. E., Cudeiro J., Davis J (1995) **Visual cortical mechanisms detecting focal orientation discontinuities** *Nature* **378**:492–6 Google Scholar

Siu C., Balsor J., Merlin S., Federer F., Angelucci A (2021) **A direct interareal feedback-to-feedforward circuit in primate visual cortex** *Nat Commun* **12**:4911 Google Scholar

Smith M. A., Kohn A (2008) **Spatial and temporal scales of neuronal correlation in primary visual cortex** *J Neurosci* **28**:12591–603 Google Scholar

Somogyi P., Cowey A (1981) **Combined Golgi and electron microscopic study on the synapses formed by double bouquet cells in the visual cortex of the cat and monkey** *J Comp Neurol* **195**:547–66 Google Scholar

Steinmetz P. N., Roy A., Fitzgerald P. J., Hsiao S. S., Johnson K. O., Niebur E (2000) **Attention modulates synchronized neuronal firing in primate somatosensory cortex** *Nature* **404**:187–90 Google Scholar

Stettler D. D., Das A., Bennett J., Gilbert C. D (2002) **Lateral connectivity and contextual interactions in macaque primary visual cortex** *Neuron* **36**:739–50 Google Scholar

Sugihara T., Qiu F. T., Von Der Heydt R. (2011) **The speed of context integration in the visual cortex** *J Neurophysiol* **106**:374–85 Google Scholar

Super H., Romeo A., Keil M (2010) **Feed-forward segmentation of figure-ground and assignment of border-ownership** *PLoS One* **5**:e10705 Google Scholar

Super H., Spekreijse H., Lamme V. A (2001) **Two distinct modes of sensory processing observed in monkey primary visual cortex (V1)** *Nat Neurosci* **4**:304–10 Google Scholar

Swindale N. V (1998) **Orientation tuning curves: empirical description and estimation of parameters** *Biol Cybern* **78**:45–56 Google Scholar

Tootell R. B., Switkes E., Silverman M. S., Hamilton S. L (1988) **Functional anatomy of macaque striate cortex. II. Retinotopic organization** *J Neurosci* **8**:1531–68 Google Scholar

Trautmann E. M., Hesse J. K., Stine G. M., Xia R., Zhu S., O'shea D. J., Karsh B., Colonell J., Lanfranchi F. F., Vyas S., Zimnik A., Amematsro E., Steinemann N. A., Wagenaar D. A., Pachitariu M., Andrei A., Lopez C. M., O'callaghan J., Putzeys J., Raducanu B. C., Welkenhuysen M., Churchland M., Moore T., Shadlen M., Shenoy K., Tsao D., Dutta B., Harris T (2025) **Large-scale high-density brain-wide neural recording in nonhuman primates** *Nat Neurosci* **28**:1562–1575 Google Scholar

Trepka E. B., Zhu S. D., Xia R. B., Chen X. M., Moore T (2022) **Functional interactions among neurons within single columns of macaque V1** *eLife* **11** Google Scholar

TS'o D. Y., Gilbert C. D., Wiesel T. N. (1986) **Relationships between horizontal interactions and functional architecture in cat striate cortex as revealed by cross-correlation analysis** *J Neurosci* **6**:1160–70 Google Scholar

Usrey W. M., Reppas J. B., Reid R. C (1998) **Paired-spike interactions and synaptic efficacy of retinal inputs to the thalamus** *Nature* **395**:384–7 Google Scholar

Van Kerkoerle T., Self M. W., Dagnino B., Gariel-Mathis M. A., Poort J., Van Der Togt C., Roelfsema P. R. (2014) **Alpha and gamma oscillations characterize feedback and feedforward processing in monkey visual cortex** *Proc Natl Acad Sci U S A* **111**:14332–41 Google Scholar

Van Kerkoerle T., Self M. W., & Roelfsema P. R. (2017) **Layer-specificity in the effects of attention and working memory on activity in primary visual cortex** *Nat Commun* **8**:13804 Google Scholar

Vangeneugden J., Van Beest E. H., Cohen M. X., Lorteije J. A. M., Mukherjee S., Kirchberger L., Montijn J. S., Thamizharasu P., Camillo D., Levelt C. N., Roelfsema P. R., Self M. W., Heimel J. A. (2019) **Activity in Lateral Visual Areas Contributes to Surround Suppression in Awake Mouse V1** *Curr Biol* **29**:4268–4275 Google Scholar

Von Der Heydt R. (2015) **Figure-ground organization and the emergence of proto-objects in the visual cortex** *Frontiers in Psychology* **6**:1695 Google Scholar

Von Der Heydt R. (2023) **Visual cortical processing—From image to object representation** *Frontiers in Computer Science* **5** Google Scholar

Von Der Heydt R., Peterhans E., Baumgartner G. (1984) **Illusory contours and cortical neuron responses** *Science* **224**:1260–2 Google Scholar

Wagatsuma N., Hu B., Von Der Heydt R., Niebur E. (2021) **Analysis of spiking synchrony in visual cortex reveals distinct types of top-down modulation signals for spatial and object-based attention** *PLoS Comput Biol* **17**:e1008829 Google Scholar

Walker G. A., Ohzawa I., Freeman R. D (1999) **Asymmetric suppression outside the classical receptive field of the visual cortex** *J Neurosci* **19**:10536–53 Google Scholar

Webb B. S., Tinsley C. J., Barraclough N. E., Parker A., Derrington A. M (2003) **Gain control from beyond the classical receptive field in primate primary visual cortex** *Vis Neurosci* **20**:221–30 Google Scholar

Williford J. R., Von Der Heydt R. (2016) **Figure-Ground Organization in Visual Cortex for Natural Scenes** *eNeuro* **3** Google Scholar

Wiser A. K., Callaway E. M (1996) **Contributions of individual layer 6 pyramidal neurons to local circuitry in macaque primary visual cortex** *J Neurosci* **16**:2724–39 Google Scholar

Xu X., Olivas N. D., Ikrar T., Peng T., Holmes T. C., Nie Q., Shi Y (2016) **Primary visual cortex shows laminar-specific and balanced circuit organization of excitatory and inhibitory synaptic connectivity** *J Physiol* **594**:1891–910 Google Scholar

Yabuta N. H., Callaway E. M (1998) **Functional streams and local connections of layer 4C neurons in primary visual cortex of the macaque monkey** *J Neurosci* **18**:9489–99 Google Scholar

Yan Y., Zhaoping L., Li W (2018) **Bottom-up saliency and top-down learning in the primary visual cortex of monkeys** *Proc Natl Acad Sci U S A* **115**:10499–10504 Google Scholar

Yoshioka T., Levitt J. B., Lund J. S (1994) **Independence and merger of thalamocortical channels within macaque monkey primary visual cortex: anatomy of interlaminar projections** *Vis Neurosci* **11**:467–89 Google Scholar

Zarella M. D., TS'o D. Y. (2016) **Cue combination encoding via contextual modulation of V1 and V2 neurons** *Eye Brain* **8**:177–193 Google Scholar

Zhang N. R., Von Der Heydt R. (2010) **Analysis of the context integration mechanisms underlying figure-ground organization in the visual cortex** *Journal of Neuroscience* **30**:6482–6496 Google Scholar

Zhang S., Xu M., Kamigaki T., Hoang Do J. P., Chang W. C., Jenvay S., Miyamichi K., Luo L., Dan Y. (2014) **Selective attention. Long-range and local circuits for top-down modulation of visual cortex processing** *Science* **345**:660–5 Google Scholar

Zhaoping L (2005) **Border ownership from intracortical interactions in visual area v2** *Neuron* **47**:143–53 Google Scholar

Zhou H., Friedman H. S., Von Der Heydt R. (2000) **Coding of border ownership in monkey visual cortex** *J Neurosci* **20**:6594–611 Google Scholar

Zhu S., Xia R., Chen X., Moore T (2024) **Comparison of orientation encoding across layers within single columns of primate V1 revealed by high-density recordings** *Front Neural Circuits* **18**:1399571 Google Scholar

Zhu S. D., Zhang L. A., Von Der Heydt R. (2020) **Searching for object pointers in the visual cortex** *Journal of Neurophysiology* **123**:1979–1994 Google Scholar

Zipser K., Lamme V. A., Schiller P. H (1996) **Contextual modulation in primary visual cortex** *J Neurosci* **16**:7376–89 Google Scholar

Author information

Shude Zhu
Department of Neurobiology and Howard Hughes Medical Institute, Stanford University School of Medicine, Stanford, United States
ORCID iD: 0000-0002-8674-9607

Yu Jin Oh
Department of Neurobiology and Howard Hughes Medical Institute, Stanford University School of Medicine, Stanford, United States

Ethan B Trepka
Department of Neurobiology and Howard Hughes Medical Institute, Stanford University School of Medicine, Stanford, United States

Xiaomo Chen
Department of Neurobiology and Howard Hughes Medical Institute, Stanford University School of Medicine, Stanford, United States, Center for Neuroscience, Department of Neurobiology, Physiology, and Behavior, UC Davis, Davis, United States
ORCID iD: 0000-0002-6142-9981

Tirin Moore
Department of Neurobiology and Howard Hughes Medical Institute, Stanford University School of Medicine, Stanford, United States

For correspondence: tirin@stanford.edu

Editors

Reviewing Editor
Supratim Ray
Indian Institute of Science Bangalore, Bengaluru, India

Senior Editor
Joshua Gold
University of Pennsylvania, Philadelphia, United States of America

Reviewer #1 (Public review):

Zhu and colleagues used high-density Neuropixel probes to perform laminar recordings in V1 while presenting either small stimuli that stimulated the classical receptive field (CRF) or large stimuli whose border straddled the RF to provide nonclassical RF (nCRF) stimulation. Their main question was to understand the relative contribution of feedforward (FF), feedback (FB), and horizontal circuits to border ownership (B_{own}), which they addressed by measuring cross-correlation across layers. They found differences in cross-correlation between feedback/horizontal (FH) and input layers during CRF and nCRF stimulation.

Comments on revisions:

In the revision, the authors have added a paragraph in the Discussion to address the question of layers 2/3 neurons leading layer 4 neurons, and have provided answers to the questions in

the public review without making substantial changes in the paper. However, there were several other recommendations, which I am not sure why were not considered. I am adding those again below.

* For CRF stimulation, the zero lag between 4C and 4A/B with layer 5/6 (Figure 3D last two columns on the right) was surprising to me. I just felt that this could be because layer 6 may also be getting FF inputs. Perhaps better not to club layer 5 with 6, as mentioned earlier also.

* Interpreting the nCRF delays, with often negative delays, was very challenging for me. For example, 4C -> 5/6 (third column in Figure 3) has a significantly negative peak (although that does not show up in statistical analysis because it seems to be a signed test to just test if the median was greater than zero, not if the median was different from zero; line 285). What is the interpretation here? Are spikes in 5/6 causing spikes in 4C (which, as mentioned earlier, would require anatomical projections from 5/6 to 4C)? On the other hand, if FB inputs arrive in 5/6 but there are no inputs going to 4C, then why should there even be a significant cross-correlation?

The only explanation I could think of is somehow an alignment of inputs in these two layers such that FH inputs come in Layer 5/6 just before FF inputs arrive in 4C, each causing a spike in a neuron in each layer which are otherwise not anatomically interconnected. But this would require both a very precise temporal coupling between FF and FH inputs arriving in these areas AND neurons in layer 5/6 which very strongly respond to FH stimulation (I thought that FH inputs are mainly modulatory and not as strong). Anyway, it would be good to see some cross correlation functions which have a negative lag (all examples in Fig 3B has positive or zero lag).

* I think cross-correlation analysis would have been useful if there was data from a feedback area (say V2). In its absence, perhaps latency analysis (by just comparing the PSTH) could have revealed something interesting, given that the hypothesis is about differences in the timings in FH versus FF inputs. Do PSTHs across layers show the type of differences that are being claimed (e.g. in line 295-297)?

* Line 262-63: "Notably, the rates were nearly identical under the two stimulus conditions" - I would have thought CRF stimulation would produce higher rates. Can the authors explain this?

* Line 174-175: Isn't the proportion of border ownership cells in layer 4C higher than one would expect under the assumption that nCRF effects are mediated by horizontal and feedback connections which layer 4C does not receive? Can authors explain?

* Figure 3D: it would also be good to show the heatmaps stacked up in the increasing order of the interelectrode distance of the pairs so that it will be easy to see how the peak lag changes with distance as well.

* It will be good to show the shift in peak lag and CCG asymmetry between CRF and nCRF conditions for the same pairs, using a violin or bar plot with lines connecting each pair in Figure 3.

* Line 594, 603, 628 and 630: What procedure was used to determine the size, location of the CRF, and optimal orientation manually online?

* Line 733-734: Although a reference is cited, please explicitly mention the rationale for keeping the peak lag cutoff at 10 ms.

* It is unclear why a grating was used for the CRF condition, instead of just having the portion of the stimulus within the RF for the nCRF condition, as the comparisons for FHi with FF are with different FF drives in each case.

* Figure 5 - the scatter is enormous, can you please provide the R2 values?

https://doi.org/10.7554/eLife.103255.2.sa3

Reviewer #2 (Public review):

Summary:

The authors present a study of how modulatory activity from outside the classical receptive field (cRF) differs from cRF stimulation. They study neural activity across the different layers of V1 in two anesthetized monkeys using Neuropixels probes. The monkeys are presented with drifting gratings and border-ownership tuning stimuli. They find that border-ownership tuning is organized into columns within V1, which is unexpected and exciting, and that the flow of activity from cell-to-cell (as judged by cross-correlograms between single units) is influenced by the type of visual stimulus: border-ownership tuning stimuli vs. drifting-grating stimuli.

Strengths:

The questions addressed by the study are of high interest, and the use of Neuropixels probes yields extremely high numbers of single-units and cross-correlation histograms (CCHs) which makes the results robust. The study is well-described.

Comments on revisions:

The results are interesting and seem robust. However, several of my main points were not addressed. The authors do not analyze or discuss the problem the border ownership stimuli do uniquely isolate feedback from feedforward influences. Here are my remaining points/recommendations:

(1) In my previous review I indicated that the border-ownership signal also provides a strong feedforward drive, a black-white edge, in addition to the border ownership signal. Calling this a "nCRF stimulus" is a misnomer. Please correct this terminology and replace it by something that is appropriate, e.g. changing it into "grating stimulation" (instead of CRF stimulation) and BO-stimulation (instead of nCRF stimulation).

(2) In my previous review I asked if the initial response for the border ownership stimulus show the feedforward signature. It is unclear to me why this suggestions did not lead to an analysis of the feedforward response. I repeat the text from my previous review: "The authors state that they did not look at cross-correlations during the initial response, but if they do, do they see the feedforward-dominated pattern? The jitter CCH analysis might suffice in correcting for the response transient." Can the authors address this point?

(3) In my previous review I asked the authors show the average time course of the response elicited by preferred and nonpreferred border ownership stimuli across all significant neurons. It remains unclear why this plot was not provided.

https://doi.org/10.7554/eLife.103255.2.sa2

Reviewer #3 (Public review):

Summary:

The paper by Zhu et al is on an important topic in visual neuroscience, the emergence in the visual cortex of signals about figure and ground. This topic also goes by the name border

ownership. The paper utilizes modern recording techniques very skillfully to extend what is known about border ownership. It offers new evidence about the prevalence of border ownership signals across different cortical layers in V1 cortex. Also, it uses pairwise cross correlation to study signal flow under different conditions of visual stimulation that include the border ownership paradigm.

Strengths: The paper's strengths are results of its use of multi-electrode probes to study border ownership in many neurons simultaneously across the cortical layers in V1. Also it provides new useful data about the dynamics of interaction of signals from the non-classical receptive field (NCRF) and the Classical receptive field (CRF).

Weaknesses:

The paper's weakness is that it does not challenge consensus beliefs about mechanisms. Also, the paper combines data about border ownership with data about the NCRF without making it clear how they are similar or different.

Critique:

The border ownership data on V1 offered in the paper replicate experimental results obtained by Zhou and von der Heydt (2000) and confirm the earlier results. The incremental addition is that the authors found border ownership in all cortical layers of V1, extending Zhou and von der Heydt's results that were only about layer 2/3 in V2 cortex. This is an interesting new result using the same stimuli but new measurement techniques.

The cross-correlation results show that the pattern of the cross correlogram (CCG) is influenced by the visual pattern being presented. However, in the initial submitted ms. the results were not analyzed mechanistically, and the interpretation was unclear. For instance, the authors show in Figure 3 (and in Figure S2) that the peak of the CCG can indicate layer 2/3 excites layer 4C when the visual stimulus is the border ownership test pattern, a large square 8 deg on a side. More than one reviewer asked, " how can layer 2/3 excite layer 4C"? . In the revised ms. the authors added a paragraph to the Discussion to respond to the reviewers about this point. The authors could provide an even better response to the reviewers by emphasizing that, consistently, layer 5/6 neurons lead neurons in layer 4, and for the CRF pattern and even more when the NCRF patterns are used.

The problems in understanding the CCG data are indirectly caused by the lack of a critical analysis of what is happening in the responses that reveal the border ownership signals, as in Fig.2. Let's put it bluntly--are border ownership signals excitatory or inhibitory? As the authors pointed out in their rebuttal, Zhang and von der Heydt (2010, JNS) did experiments to answer this question but I do not agree with the authors rebuttal letter about what Zhang and von der Heydt (2010) reported. If you examine Zhang and von der Heydt's Figure 6, you see that the major effect of stimulating border ownership neurons is suppression from the non-preferred side. That result is consistent with many papers on the NCRF (many cited by the authors) that indicate that it is mostly suppressive. That experimental fact about border ownership should be mentioned in the present paper.

What I should have pointed out in the first round, but didn't understand it then, is that there is a disconnect between the the border ownership laminar analysis (Figure 2) and the laminar correlations with CCGs (Figures 3-5) because the CCGs are not limited to border ownership neurons (or at least we are not told they were limited to them). So the CCG results are not mostly about border ownership--they are about the difference between signal flow in responses to small drifting Gabor patterns vs big flashed squares. Since only 21% of all recorded neurons were border ownership neurons, it is likely that most of the CCG statistics is based on neurons that do not show border ownership. Nevertheless, Figures 3 and 4 are very useful for the study of signal flow in the NCRF. It wasn't clear to me and I think the authors could make it clearer what those figures are about.

And I wonder if it might be possible to make a stronger link with border ownership by restricting the CCG analysis to pairs of neurons in which one neuron is a border ownership neuron. Are there enough data?

My critique of the CCG analysis applies to Figure 5 also. That figure shows a weak correlation of CCG asymmetry with Border Ownership Index. Perhaps a stronger correlation might be present if the population were restricted to the much smaller population of neuron pairs that had at least one border ownership neuron.

https://doi.org/10.7554/eLife.103255.2.sa1

Author response:

The following is the authors' response to the original reviews.

> ***Reviewer #1 (Public review):***
>
> *Zhu and colleagues used high-density Neuropixel probes to perform laminar recordings in V1 while presenting either small stimuli that stimulated the classical receptive field (CRF) or large stimuli whose border straddled the RF to provide nonclassical RF (nCRF) stimulation. Their main question was to understand the relative contribution of feedforward (FF), feedback (FB), and horizontal circuits to border ownership (Bown), which they addressed by measuring crosscorrelation across layers. They found differences in cross-correlation between feedback/horizontal (FH) and input layers during CRF and nCRF stimulation.*
>
> *Although the data looks high quality and analyses look mostly fine, I had a lot of difficulty understanding the logic in many places. Examples of my concerns are written below.*
>
> *(1) What is the main question? The authors refer to nCRF stimulation emerging from either feedback from higher areas or horizontal connections from within the same area (e.g. lines 136 to 138 and again lines 223-232). I initially thought that the study would aim to distinguish between the two. However, the way the authors have clubbed the layers in 3D, the main question seems to be whether Bown is FF or FH (i.e., feedback and horizontal are clubbed). Is this correct? If so, I don't see the logic, since I can't imagine Bown to be purely FF. Thus, just showing differences between CRF stimulation (which is mainly expected to be FF) and nCRF stimulation is not surprising to me.*

We thank the reviewer for their thoughtful comments. As explained in the discussion, we grouped cortical layers to reduce uncertainty in precisely assigning laminar boundaries and to increase statistical power. Consequently, this limits our ability to distinguish the relative contributions of feedback inputs, primarily targeting layers 1 and 6, and horizontal connections, mainly within layers 2/3 and 5. Nevertheless, previous findings, especially regarding the rapid emergence of B_{own} signals, suggest that feedback is more biologically plausible than horizontal-based mechanisms.

Importantly, the emergence of B_{own} signals in the primate brain should not be taken for granted. Direct physiological evidence that distinguishes feedforward from feedback/horizontal mechanisms has been lacking. While we agree it is unlikely that B_{own} is mediated solely by feedforward processing, we felt it was necessary to test this empirically, particularly using highresolution laminar recordings.

As discussed, feedforward models of B_{own} have been proposed (e.g., Super, Romeo, and Keil, 2010; Saki and Nishimura, 2006). These could, in theory, be supported by more general nCRF

modulations arising through early feedforward inhibitions, such as those observed in the retinogeniculate pathway (e.g., Webb, Tinsley, Vincent and Derrington, 2005; Blitz and Regehr, 2005; Alitto and Usrey, 2008). However, most B_{own} models rely heavily on response latency, yet very few studies have recorded across layers or areas simultaneously to address this directly. Notably, recent findings in area V4 show that B_{own} signals emerge earlier in deep layers than in granular (input) layers, suggesting a non-feedforward origin (Franken and Reynolds, 2021).

Furthermore, although previous studies have shown that the nCRF can modulate firing rates and the timing of neuronal firing across layers, our findings go beyond these effects. We provide clear evidence that nCRF modulation also alters precise spike timing relationships and interlaminar coordination, and that the magnitude of nCRF modulation depends on these interlaminar interactions. This supports the idea that B_{own} , or more general nCRF modulation, involves more than local rate changes, reflecting layer-specific network dynamics consistent with feedback or lateral integration.

> *(2) Choice of layers for cross-correlation analysis: In the Introduction, and also in Figure 3C, it is mentioned that FF inputs arrive in 4C and 6, while FB/Horizontal inputs arrive at "superficial" and "deep", which I take as layer 2/3 and 5. So it is not clear to me why (i) layer 4A/B is chosen for analysis for Figure 3D (I would have thought layer 6 should have been chosen instead) and (ii) why Layers 5 and 6 are clubbed.*

We thank the reviewer for raising this important point. The confusion likely stems from our use of the terms “superficial” and “deep” layers when describing the targets of feedback/horizontal inputs. To clarify, by “superficial” and “deep,” we specifically refer to layers 1–3 and layers 5–6, respectively, as illustrated in Figure 3C. Feedback and horizontal inputs relatively avoid entire layer 4, including both 4C and 4A/B.

We also emphasize that the classification of layers as feedforward or feedback/horizontal recipients is relative rather than absolute. For example, although layer 6 receives both feedforward and feedback/horizontal inputs, it contains a higher proportion of feedback/horizontal inputs compared to layers 4C and 4A/B.

We had addressed this rationale in the Discussion, but recognize it may not have been sufficiently emphasized. We have revised the main text accordingly to clarify this point for readers in the final manuscript version.

> *(3) Addressing the main question using cross-correlation analysis: I think the nice peaks observed in Figure 3B for some pairs show how spiking in one neuron affects the spiking in another one, with the delay in cross-correlation function arising from the conduction delay. This is shown nicely during CRF stimulation in Figure 3D between 4C -> 2/3, for example. However, the delay (positive or negative) is constrained by anatomical connectivity. For example, unless there are projections from 2/3 back to 4C which causes firing in a 2/3 layer neuron to cause a spike in a layer 4 neuron, we cannot expect to get a negative delay no matter what kind of stimulation (CRF versus nCRF) is used.*

We thank the reviewer for the insightful comment. The observation that neurons within FH_i laminar compartments (layers 2/3, 5/6) can lead those in layer 4 (4C, 4A/B) during nCRF stimulation may indeed seem unexpected. However, several anatomical pathways could mediate the propagation of B_{own} signals from FH_i compartments to layer 4. We have revised the Discussion section in the final version of the manuscript to address this point explicitly.

In Macaque V1, projections from layers 2/3 to 4A/B have been documented (Blasdel et al., 1985; Callaway and Wiser, 1996), and neurons in 4A/B often extend apical dendrites into layers 2/3 (Lund, 1988; Yoshioka et al., 1994). Although direct projections from layers 2/3 to 4C

are generally sparse (Callaway, 1998), a subset of neurons in the lower part of layer 3 can give off collateral axons to 4C (Lund and Yoshioka, 1991). Additionally, some 4C neurons extend dendrites into 4B, enabling potential dendritic integration of inputs from more superficial layers (Somogyi and Cowey, 1981; Mates and Lund, 1983; Yabuta and Callaway, 1998). Sparse connections from 2/3 to layer 4 have also been reported in cat V1 (Binzegger, Douglas and Martin, 2004). Moreover, layers 2/3 may influence 4C neurons disynaptically, without requiring dense monosynaptic connections.

Importantly, while CCGs can suggest possible circuit arrangements, functional connectivity may arise through mechanisms not fully captured by traditional anatomical tracing. Indeed, the apparent discrepancy between anatomical and functional data is not uncommon. For example, although 4B is known to receive anatomical input primarily from 4Cα, but not 4Cβ, photostimulation experiments have shown that 4B neurons can also be functionally driven by 4Cβ (Sawatari and Callaway, 1996). Our observation of functional inputs from layers 2/3 to layer 4 is also consistent with prior findings in rodent V1, where CCG analysis (e.g., Figure 7 in Senzai, Fernandez-Ruiz and Buzsaki, 2019) or photostimulation (Xu et al., 2016) revealed similar pathways.

Layers 5/6 provide dense projections to layers 4A/B (Lund, 1988; Callaway, 1998). In particular, layer 6 pyramidal neurons, especially the subset classified as Type 1 cells, project substantially to layer 4C (Wiser and Callaway, 1996; Fitzpatrick et al., 1985).

> ***Reviewer #2 (Public review):***
>
> *Summary:*
>
> *The authors present a study of how modulatory activity from outside the classical receptive field (cRF) differs from cRF stimulation. They study neural activity across the different layers of V1 in two anesthetized monkeys using Neuropixels probes. The monkeys are presented with drifting gratings and border-ownership tuning stimuli. They find that border-ownership tuning is organized into columns within V1, which is unexpected and exciting, and that the flow of activity from cellto-cell (as judged by cross-correlograms between single units) is influenced by the type of visual stimulus: border-ownership tuning stimuli vs. drifting-grating stimuli.*
>
> *Strengths:*
>
> *The questions addressed by the study are of high interest, and the use of Neuropixels probes yields extremely high numbers of single-units and cross-correlation histograms (CCHs) which makes the results robust. The study is well-described.*
>
> *Weaknesses:*
>
> *The weaknesses of the study are (a) the use of anesthetized animals, which raises questions about the nature of the modulatory signal being measured and the underlying logic of why a change in visual stimulus would produce a reversal in information flow through the cortical microcircuit and (b) the choice of visual stimuli, which do not uniquely isolate feedforward from feedback influences.*
>
> *(1) The modulation latency seems quite short in Figure 2C. Have the authors measured the latency of the effect in the manuscript and how it compares to the onset of the visually driven response? It would be surprising if the latency was much shorter than 70ms given previous measurements of BO and figure-ground modulation latency in V2 and V1. On the same note, it might be revealing to make laminar profiles of the modulation (i.e. preferred - non-preferred border orientation) as it develops over time. Does the modulation start in feedback recipient layers?*

> *(2) Can the authors show the average time course of the response elicited by preferred and nonpreferred border ownership stimuli across all significant neurons?*

We thank the reviewer for the insightful comment—this is indeed an important and often overlooked point. As noted in the Discussion, B_{own} modulation differs from other forms of figure-ground modulation (e.g., Lamme et al., 1998) in that it can emerge very rapidly in early visual cortex—within ~10–35 ms after response onset (Zhou et al., 2000; Sugihara et al., 2011). This rapid emergence has been interpreted as evidence for the involvement of fast feedback inputs, which can propagate up to ten times faster than horizontal connections (Girard et al., 2001). Moreover, interlaminar interactions via monosynaptic or disynaptic connections can occur on very short timescales (a few milliseconds), further complicating efforts to disentangle feedback influences based solely on latency.

Thus, while the early onset of modulation in our data may appear surprising, it is consistent with prior B_{own} findings, and likely reflects a combination of fast feedback and rapid interlaminar processing. This makes it challenging to use conventional latency measurements to resolve laminar differences in B_{own} modulation. Latency comparisons are well known to be susceptible to confounds such as variability in response onset, luminance, contrast, stimulus size, and other sensory parameters.

Although we did not explicitly quantify the latency of B_{own} modulation in this manuscript, our cross-correlation analysis provides a more sensitive and temporally resolved measure of interlaminar information flow. We therefore focused on this approach rather than laminar modulation profiles, as it more directly addresses our primary research question.

> *(3) The logic of assuming that cRF stimulation should produce the opposite signal flow to borderownership tuning stimuli is worth discussing. I suspect the key difference between stimuli is that they used drifting gratings as the cRF stimulus, the movement of the stimulus continually refreshes the retinal image, leading to continuous feedforward dominance of the signals in V1. Had they used a static grating, the spiking during the sustained portion of the response might also show more influence of feedback/horizontal connections. Do the initial spikes fired in response to the borderownership tuning stimuli show the feedforward pattern of responses? The authors state that they did not look at cross-correlations during the initial response, but if they do, do they see the feedforward-dominated pattern? The jitter CCH analysis might suffice in correcting for the response transient.*

We thank the reviewer for the insightful comment. As noted in the final Results section, our CRF and nCRF stimulation paradigms differ in respects beyond the presence or absence of nonclassical modulation, including stimulus properties within the CRF.

We agree with the reviewer's speculation that drifting gratings may continually refresh the retinal image, promoting sustained feedforward dominance in V1, whereas static gratings might allow greater influence from feedback/horizontal inputs during the sustained response. Likewise, the initial response to the B_{own} stimulus could be dominated by feedforward activity before feedback/horizontal influences arrive.

This contrast was a central motivation for our experimental design: we deliberately used two stimulus conditions — drifting gratings to emphasize feedforward processing, and B_{own} stimuli, which are known to engage feedback modulation — to test whether these two conditions yield different patterns of interlaminar information flow. Our results confirm that they do. While we did not separately analyze the very initial spike period, our focus is on interlaminar information flow during the sustained response, which serves as the primary measure of feedback/horizontal engagement in this study.

Finally, beyond this direct comparison, we show in Figure 5 that under nCRF stimulation alone, the direction and strength of interlaminar information flow correlate with the magnitude of B_{own} modulation, further supporting the idea that our cross-correlation approach reveals functionally meaningful differences in cortical processing.

> *(4) The term "nCRF stimulation" is not appropriate because the CRF is stimulated by the light/dark edge.*

We thank the reviewer for the comment. As noted in the Introduction, nCRF effects described in the literature invariably involve stimulation both inside and outside the CRF. Our use of the term “nCRF stimulation” refers to this experimental paradigm, rather than suggesting that the CRF itself is unstimulated. We hope this clarifies our use of the term.

> ***Reviewer #3 (Public review):***
>
> *Summary:*
>
> *The paper by Zhu et al is on an important topic in visual neuroscience, the emergence in the visual cortex of signals about figures and ground. This topic also goes by the name border ownership. The paper utilizes modern recording techniques very skillfully to extend what is known about border ownership. It offers new evidence about the prevalence of border ownership signals across different cortical layers in V1 cortex. Also, it uses pairwise cross-correlation to study signal flow under different conditions of visual stimulation that include the border ownership paradigm.*
>
> *Strengths:*
>
> *The paper's strengths are its use of multi-electrode probes to study border ownership in many neurons simultaneously across the cortical layers in V1, and its innovation of using crosscorrelation between cortical neurons -- when they are viewing border-ownership patterns or instead are viewing grating patterns restricted to the classical receptive field (CRF).*
>
> *Weaknesses:*
>
> *The paper's weaknesses are its largely incremental approach to the study of border ownership and the lack of a critical analysis of the cross-correlation data. The paper as it is now does not advance our understanding of border ownership; it mainly confirms prior work, and it does not challenge or revise consensus beliefs about mechanisms. However, it is possible that, in the rich dataset the authors have obtained, they do possess data that could be added to the paper to make it much stronger.*
>
> *Critique:*
>
> *The border ownership data on V1 offered in the paper replicates experimental results obtained by Zhou and von der Heydt (2000) and confirms the earlier results using the same analysis methods as Zhou. The incremental addition is that the authors found border ownership in all cortical layers extending Zhou's results that were only about layer 2/3.*
>
> *The cross-correlation results show that the pattern of the cross-correlogram (CCG) is influenced by the visual pattern being presented. However, the results are not analyzed mechanistically, and the interpretation is unclear. For instance, the authors show in Figure 3 (and in Figure S2) that the peak of the CCG can indicate layer 2/3 excites layer 4C when the visual stimulus is the border ownership test pattern, a large square 8 deg on a side. But how can layer 2/3 excite layer 4C? The authors do not raise or offer an answer*

> *to this question. Similar questions arise when considering the CCG of layer 4A/B with layer 2/3. What is the proposed pathway for layer 2/3 to excite 4A/B? Other similar questions arise for all the interlaminar CCG data that are presented. What known functional connections would account for the measured CCGs?*

We thank the reviewer for raising this important point. As noted in our response to a previous comment, several anatomical pathways could mediate apparent functional inputs from layers 2/3 to 4C and 4A/B. In macaque V1, projections from layers 2/3 to 4A/B have been documented (Blasdel et al., 1985; Callaway and Wiser, 1996), and neurons in 4A/B often extend apical dendrites into layers 2/3 (Lund, 1988; Yoshioka et al., 1994). Although direct projections from layers 2/3 to 4C are generally sparse (Callaway, 1998), a subset of lower layer 3 neurons can give off collateral axons to 4C (Lund and Yoshioka, 1991). Some 4C neurons also extend dendrites into 4B, potentially allowing dendritic integration of inputs from more superficial layers (Somogyi and Cowey, 1981; Mates and Lund, 1983; Yabuta and Callaway, 1998). Sparse connections from 2/3 to layer 4 have also been reported in cat V1 (Binzegger et al., 2004).

Moreover, layers 2/3 may influence 4C neurons disynaptically, without requiring dense monosynaptic connections. While CCGs suggest possible circuit arrangements, functional connectivity may arise through mechanisms not fully captured by anatomical tracing, and apparent discrepancies between anatomical and functional data are not uncommon. For example, although 4B is known to receive anatomical input primarily from 4Cα, 4B neurons can also be functionally driven by 4Cβ using photostimulation (Sawatari and Callaway, 1996). Our observation of functional inputs from layers 2/3 to layer 4 is also consistent with prior findings in rodent V1, where CCG analysis (e.g., Figure 7 in Senzai, Fernandez-Ruiz and Buzsaki, 2019) or photostimulation (Xu et al., 2016) revealed similar pathways.

Layers 5/6 also provide dense projections to layers 4A/B (Lund, 1988; Callaway, 1998). In particular, layer 6 pyramidal neurons, especially the subset classified as Type 1 cells, project substantially to layer 4C (Wiser and Callaway, 1996; Fitzpatrick et al., 1985).

We have revised the Discussion section to explicitly address these points and clarify the potential anatomical and functional pathways underlying the measured interlaminar CCGs, highlighting how inputs from layers 2/3 and 5/6 to layer 4 can be mediated via both direct and indirect connections.

> *The problems in understanding the CCG data are indirectly caused by the lack of a critical analysis of what is happening in the responses that reveal the border ownership signals, as in Figure 2. Let's put it bluntly - are border ownership signals excitatory or inhibitory? The reason I raise this question is that the present authors insightfully place border ownership as examples of the action of the non-classical receptive field (nCRF) of cortical cells. Most previous work on the nCRF (many papers cited by the authors) reveal the nCRF to be inhibitory or suppressive. In order to know whether nCRF signals are excitatory or inhibitory, one needs a baseline response from the CRF, so that when you introduce nCRF signals you can tell whether the change with respect to the CRF is up or down. As far as I know, prior work on border ownership has not addressed this question, and the present paper doesn't either. This is where the rich dataset that the present authors possess might be used to establish a fundamental property of border ownership.*
>
> *Then we must go back to consider what the consequences of knowing the sign of the border ownership signal would mean for interpreting the CCG data. If the border ownership signals from extrastriate feedback or, alternatively, from horizontal intrinsic connections, are excitatory, they might provide a shared excitatory input to pairs of cells that would show up in the CCG as a peak at 0 delay. However, if the border ownership manuscript signals are inhibitory, they might work by exciting only inhibitory neurons in*

> *V1. This could have complicated consequences for the CCG.The interpretation of the CCG data in the present version of the m is unclear (see above). Perhaps a clearer interpretation could be developed once the authors know better what the border ownership signals are.*

We thank the reviewer for raising this fundamental and thought-provoking question. As noted, B_{own} signals arise from nCRF, which has often been associated with suppressive effects. However, Zhang and von der Heydt (2010) provided important insight into this issue by systematically varying the placement of figure fragments outside the CRF while keeping an edge centered within the CRF. They found that contextual fragments on the preferred side of B_{own} produce facilitation, while those on the non-preferred side produce suppression. Thus, the nCRF contribution to B_{own} reflects both excitatory and inhibitory modulation, depending on the spatial configuration of the figure.

These effects were well explained by their model in which feedback from grouping cells in higher areas selectively enhances or suppresses V1/V2 neuron responses, depending on their B_{own} preference. In this framework, the B_{own} signal itself is not inherently excitatory or inhibitory; rather, it results from the net effect of feedback, which can be either facilitative or suppressive. Importantly, it is the input that is modulated — not that the receiving neurons are necessarily inhibitory themselves.

In the current study, our analysis focused on CCGs showing excessive coincident spiking, i.e., positive peaks, which are typically interpreted as evidence for shared excitatory input or excitatory connections. Due to the limited number of connections, we did not analyze inhibitory interactions, such as anti-correlations or delayed suppression in the CCGs, which would be expected if the reference neuron were inhibitory. Therefore, the CCGs we report here likely reflect the excitatory component of the B_{own} signal, and possibly its upstream drive via feedback. While a full separation of excitatory and inhibitory components remains an important goal for future work, our data suggest that B_{own} modulation is at least partially mediated through excitatory feedback input.

> *My critique of the CCG analysis applies to Figure 5 also. I cannot comprehend the point of showing a very weak correlation of CCG asymmetry with Border Ownership Index, especially when what CCG asymmetry means is unclear mechanistically. Figure 5 does not make the paper stronger in my opinion.*

We thank the reviewer for this comment. As described in the Results section for Figure 5, the observation that interlaminar information flow correlates with B_{own} modulation is important because it demonstrates that these flow patterns are specifically related to the magnitude of B_{own} signals, independent of the comparisons between CRF and nCRF stimulation.

> *In Figure 3, the authors show two CCGs that involve 4C--4C pairs. It would be nice to know more about such pairs. If there are any 6--6 pairs, what they look like also would be interesting. The authors also in Figure 3 show CCG's of two 4C--4A/B pairs and it would be quite interesting to know how such CCGs behave when CRF and nCRF stimuli are compared. In other words, the authors have shown us they have many data but have chosen not to analyze them further or to explain why they chose not to analyze them. It might help the paper if the authors would present all the CCG types they have. This suggestion would be helpful when the authors know more about the sign of border ownership signals, as discussed at length above.*

We thank the reviewer for the insightful comment. The rationale for selecting specific laminar pairs is described in the Results section after Figure 3C and further discussed in the Discussion. In brief, we focused on CCGs computed from pairs in which one neuron resided

in laminar compartments receiving feedback/horizontal inputs (layers 2/3 and 5/6) and the other within compartments relatively devoid of these inputs (layers 4C and 4A/B).

To mitigate uncertainty in defining exact laminar boundaries and to maximize statistical power, we combined some anatomical layers into distinct laminar compartments. This approach allowed us to compare the relative spike timing between neuronal pairs during CRF and nCRF stimulation. If feedback/horizontal inputs contribute more during nCRF than CRF stimulation, we expect this to be reflected in the lead-lag relationships of the CCGs. While other pairs (e.g., 5/6–5/6 or 4C– 4A/B) could in principle be analyzed, the hypothesized patterns for these pairs are less clear, and thus they were not the focus of our study. Nonetheless, these additional pairs represent interesting directions for future work.

https://doi.org/10.7554/eLife.103255.2.sa0